Variations in Acoustic Properties of Near Surface Sediments and the Effects on High Resolution Seismic Data Evaluated by Laboratory Tests, In-situ Measurements, and Seismic Modelling

Nörmark, E; Thorsen, Grete; Lykke-Andersen, Holger

Publication date:
1996

Document Version
Early version, also known as pre-print

AAU Geotechnical Engineering Papers ISSN 1398-6465 R 9609

Variations in acoustic properties of near surface sediments and the effects on high resolution seismic data evaluated by laboratory tests, in-situ measurements, and seismic modelling

E. Nörmark, G. Thorsen, H. Lykke-Andersen

1996 Engineering Geology Paper No 2

GEOTECHNICAL ENGINEERING GROUP
AALBORG UNIVERSITY DENMARK

Nörmark, E., Thorsen, G., Lykke-Andersen, H. (1996). Variations in acoustic properties of near surface sediments and the effects on high resolution seismic data evaluated by laboratory tests, in-situ measurements, and seismic modelling. (LITASEIS).

AAU Geotechnical Engineering Papers, ISSN 1398-6465 R9609.

Engineering Geology Paper No 2

The paper has been published in *Deutsche Wissenschaftliche Gesellschaft für Erdöl, Erdgas und Kohle e.V. DGMK Forschungsbericht 397-2/1,* pp. 77-128.

The **A**AU **G**eotechnical **E**ngineering **P**apers - AGEP - are issued for early dissemination and book keeping of research results from the Geotechnical Engineering Group at Aalborg University (Department of Civil Engineering). Moreover, the papers accommodate proliferation and documentation of field and laboratory test series not directly suited for publication in journals or proceedings.

The papers are numbered ISSN 1398-6465 R<two digit year code><two digit consecutive number>. For internal purposes the papers are, further, submitted with coloured covers in the following series:

Series	Colour
Laboratory testing papers	sand
Field testing papers	grey
Manuals & guides	red
Soil Mechanics papers	blue
Foundation Engineering papers	green
Engineering Geology papers	yellow
Environmental Engineering papers	brown

In general the AGEP papers are submitted to journals, conferences or scientific meetings and hence, whenever possible, reference should be given to the final publication (journal, proceeding etc.) and not to the AGEPpaper.

3. Variations in acoustic properties of near surface sediments and the effects on high resolution seismic data evaluated by laboratory tests, in-situ measurements, and seismic modelling

E. Nörmark, G. Thorsen und H. Lykke-Andersen

Abstract

Two shallow reflection seismic data sets, acquired in areas with unconsolidated surface sediments, demonstrate that severe variations in the data quality can be expected in such places. At a locality in Northern Jutland, Denmark, laboratory tests on undisturbed samples have been conducted. The results indicate that in spite of fairly constant elastic properties, in terms of Young's modulus and shear modulus, highly variable seismic reflections are observed, which are mainly expressed in the spectral variations of high frequency signals.

It is demonstrated that absorption plays a major role for the spectral variations and that potential fluctuations in the source signals are only of secondary importance. The P-wave attenuation has been estimated from resonance column tests, VSP experiments, and seismic modelling, and the S-wave attenuation has been determined by monitoring the direct wave in hollow auger drill stem as function of depth by a new technique developed under the present project. These experiments indicate that severe attenuation in thin layers of high frequency signals occurs. Low frequency signals are not affected as much as could be expected, probably due to the fact that absorption takes place over short intervals.

The surface intervals where severe attenuation of high frequency signals are observed correlate with the presence of methane gas, which is detected at depths between 3 m and 13 m by continuous gas soundings with cone penetration equipment. The gas is mainly present in thin layers between 0.5 m and 1.0 m thick.

A spectral modelling procedure aimed at layered absorbing media has also been developed, which is used for modelling shallow reflections. Special feature in the present modelling technique is the ability to suppress period effects induced by the discrete Fourier transformation. The suppression of wrap-around effects is achieved by seeking a solution with an exponential damping in time and space, which can be fully compensated for after Fourier transformation to the time-space domain.

1 Introduction

Shallow reflection seismic data acquired in areas with surface layers consisting of unconsolidated sediments are often characterized by a highly variable data quality. This has been experienced during several shallow seismic surveys conducted in Denmark in recent years by Department of Earth Sciences, Aarhus University. The variations in data quality are most pronounced for land seismic data and are mainly expressed in spectral variations. Many factors affect the spectral content of stacked data such as statics, the conditions near the shot point, the saturation of the near surface sediments, and the lithological variations affecting the acoustic properties of sediments. The variations in data quality has in particular been observed on shallow seismic data, but are also valid for conventional seismic data, although less pronounced.

The motivation for the present project was to uncover the main reason for these variations in the reflection seismic data. It is our impression that lithological properties are of main importace for these variations. Therefore, we focussed our attention on these properties and searched for a place where the influences from other factors were negligible. The choice fell on a locality in Northern Jutland, Denmark, where significant variations in shallow seismic data had previously been observed. In order to demonstrate the variation in data quality a reflection seismic profile was acquired with densely spaced source and receiver points. The acquisition and processing of this profile will be described in the following section. Another shallow seismic profile, where several other factors affect the data quality, will be shown for comparison.

In order to describe the lithological properties of the sediments on our main locality two wells have been established, and undisturbed samples have been extracted mainly for geotechnical experiments. These are resonant column measurements for estimating Young's modulus and bender element tests for determining the shear modulus. Also undisturbed samples have been taken along the seismic profile at 2 m depth, which have been analyzed as well. Beside geotechnical description the samples have been dated and described geologically. Furthermore, cone penetration tests have been conducted along the profile to depths between 8 m and 24 m for determining the structures of the uppermost sediments, which could not be evaluated from the reflection seismic data. A geological description is compiled in section 3, and the results of the geotechnical experiments are given in section 4 and 5. In order to confirm or deny the presence of gas in the sediments continuous gas soundings have been accomplished by use of cone penetration equipment. These soundings are analyzed in section 6.

The relationship between the geotechnical measurements and the seismic experiments has been established through a number of seismic in-situ measurements. These comprise VSP measurements, S-wave refraction measurements, and vertical monitoring of the direct S-wave signals for estimating the S-wave attenuation.

Finally, a modelling program for estimating synthetic seismograms in models with horizontal layering has been developed. The modelling is based on a spectral wavefield estimation in the frequency-wavenumber domain. Such modelling routines make it relatively uncomplicated to include absorption and dispersion into the wavefield estimation. Special feature in the present modelling technique is the ability to suppress wrap-around effects, so that relatively short periods can be used in the wavefield modelling. The modelling routine has been used for calculating synthetic seismograms based on the elastic parameters estimated from the laboratory tests and the seismic in-situ measurements.

2 Shallow reflection seismic data

A shallow seismic survey from the southern part of Jutland

First, an example of typical variations in shallow reflection seismic data acquired in areas with unconsolidated surface sediments will be presented. According to our experiences the present data are fairly representative for shallow seismic data acquired under Danish conditions. The seismic data have been recorded in Holsted in the southern part of Jutland for Sønderjylland's Amt and Kort- og Matrikelstyrelsen. The main purpose of the present survey was to map the extent and the depth of a "buried valley" filled with Quaternary deposits.

For recordings 50 g and 100 g dynamite charges have been used which were activated at 2 m depth in mainly sandy deposits. The dynamite used (which are manufactured under the name Maxiprime) is supposed to have a very fast ignition, which was expected to give a wider source spectrum compared to conventional dynamite. However, this did not cause any significant improvement in the data quality. The acquisition was made on 26 channels with a geophone spacing of 5 m and a shot point interval of 5 m and 10 m, resulting in 6 and 12 fold seismic data. An end-on configuration with a minimum offset varying between 25 m and 95 m was used.

A traditional processing has been applied to the data. First, a low-cut filter between 30 Hz and 50 Hz is used, which has suppressed part of the surface waves, but not enough to recover reflections in the time-offset range most severely affected by ground roll. The remaining surface waves has removed by surgical mute. A front mute has also been applied to eliminate the direct P-wave. Subsequently, the velocity analysis and the residual static corrections have been carried out. These processes have been repeated several times in order to improve the results. Part of the stacked seismic section is shown in Fig. 2.1, on which a 50 Hz - 150 Hz bandpass filter and a trace mix over 3 traces with weights 1,4,1 has been applied.

The variations in the data quality along the present shallow seismic profile are influenced by several factors. The source signals are affected by shots in different material, and variations in the surface elevations along the profile have caused shots in both partially and fully saturated material. Moreover, the expected variations in the elastic properties have affected

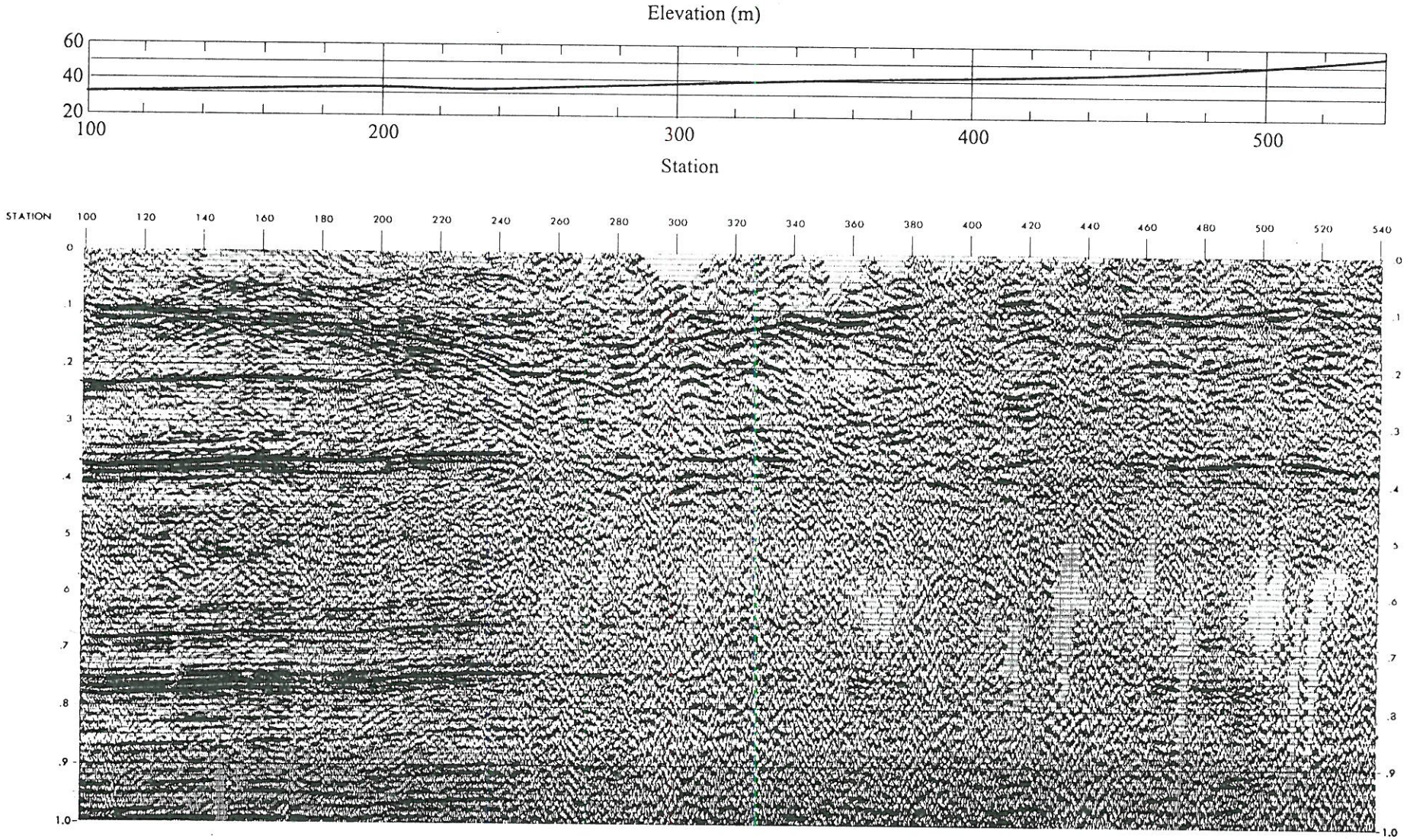

Fig. 2.1. Part of the shallow reflection seismic profile acquired near Holsted in the southern part of Jutland.

the wave propagation. Finally, in some intervals statics may not have been fully compensated for, due to lack of information about velocities and thiknesses of the surface layers and due to the fact that the reflected signals are too weak for a reliable residual static estimation.

For comparison conventional seismic data acquired by Western Geophysical near the shallow seismic profile is shown in Fig. 2.2. Recordings have been made with shots at 1 kg and at shot depths of 18 m. It is observed that by using bigger charge sizes at greater shot depth the same severe variations in data quality, that have were present on the shallow seismic data are greatly avoided. Yet, weaker reflections can still be observed under the central parts of the buried valley (as for instance for the reflection at 400 ms two-way traveltime at sta. 300) compared to the same reflection outside this interval. When making such comparisons it should be emphasized that recording geometry favours the present conventional data, due to the fact that a receiver array with more geophones is used, and because more channels and a greater spread length are applied giving a higher coverage compared to the shallow seismic data.

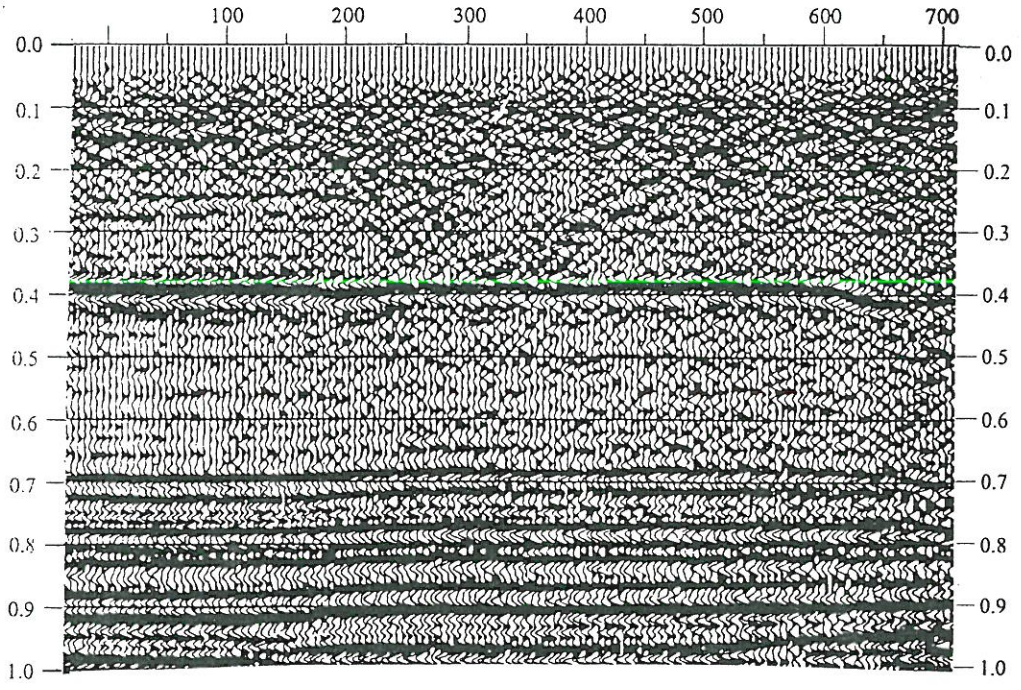

Fig. 2.2. Part of line DCJ-009 acquired by Western Geophysical. The positions have been projected into the shallow seismic line and station numbers for that profile are annotated.

The present data examples have demonstrated, that when acquiring reflection seismic data in areas with unconsolidated surface sediments, severe variations in the data quality can be expected on shallow seismic data. Conventional seismic data have not been affected to the same extent, although some reduction in the reflection strength can be observed in the most critical intervals where the highest attenuation can be expected. This is observed in spite of the fact that source and recording configuration in conventional surveys has been designed to avoid these potential problems.

Shallow seismic data from the Nr. Lyngby locality

In order to isolate the lithological effect from other potential sources to the deterioration of seismic reflections a locality in the northern part of Jutland has been selected, where it was expected that the elastic properties and the character of the sediments in general were the only factors having a significant impact on the data quality. The locality for which the position is shown in Fig. 2.3 is on the beach near the shore line. Thus the recording elevation was virtually zero. The locality is characterized by a severe erosion, which in the latest centuries have removed more than 1.0 m of the shore per year. Therefore, it is reasonable to assume that only the sediments very close to the surface consist of recently redeposited material. The cone penetration tests, which will be described in section 5, suggest that only the uppermost 1.0 m consists of recently reworked sand.

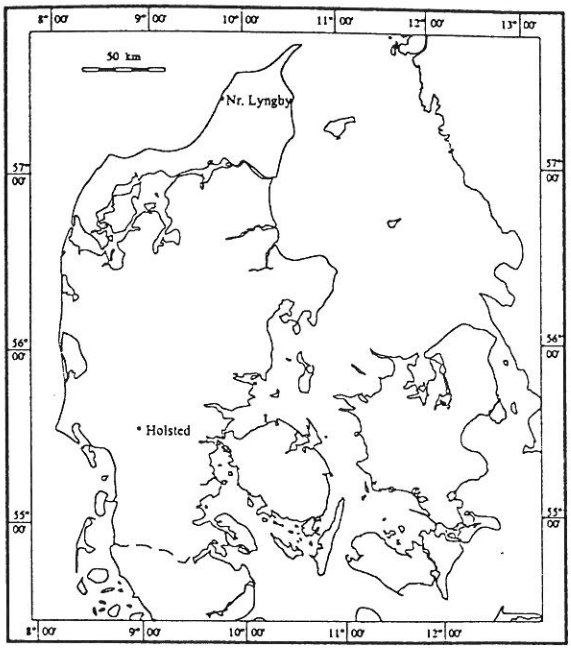

Fig. 2.3 Regional map showing the position of the main locality at Nr. Lyngby in Northern Jutland. Also the locality mentioned previously is indicated.

Since the area is virtually at elevation zero, all recordings could be made under fully water saturated conditions. Consequently, the variations in source signals cannot be expected to be as severe as for the previous seismic example, where shots were made under both saturated and unsaturated conditions. Moreover, it is unlikely that significant statics problems are present. The remaining potential effects to variations in the data quality may be caused by differences in source signals and variations in the ability of the sediments to transmit the seismic signals.

A seismic profile acquired in 1986 indicates that significant variations in the data quality is present, cf. Fig. 2.4. Charge sizes of 25 g have been used in this survey. The shot point interval and the receiver spacing compare to the recording parameters applied in the seismic survey from the southern part of Jutland, for which the stacked data are presented above. On these data it should be noted that between station 300 and 400 significantly lower frequencies are observed compared to the reflections outside this interval.

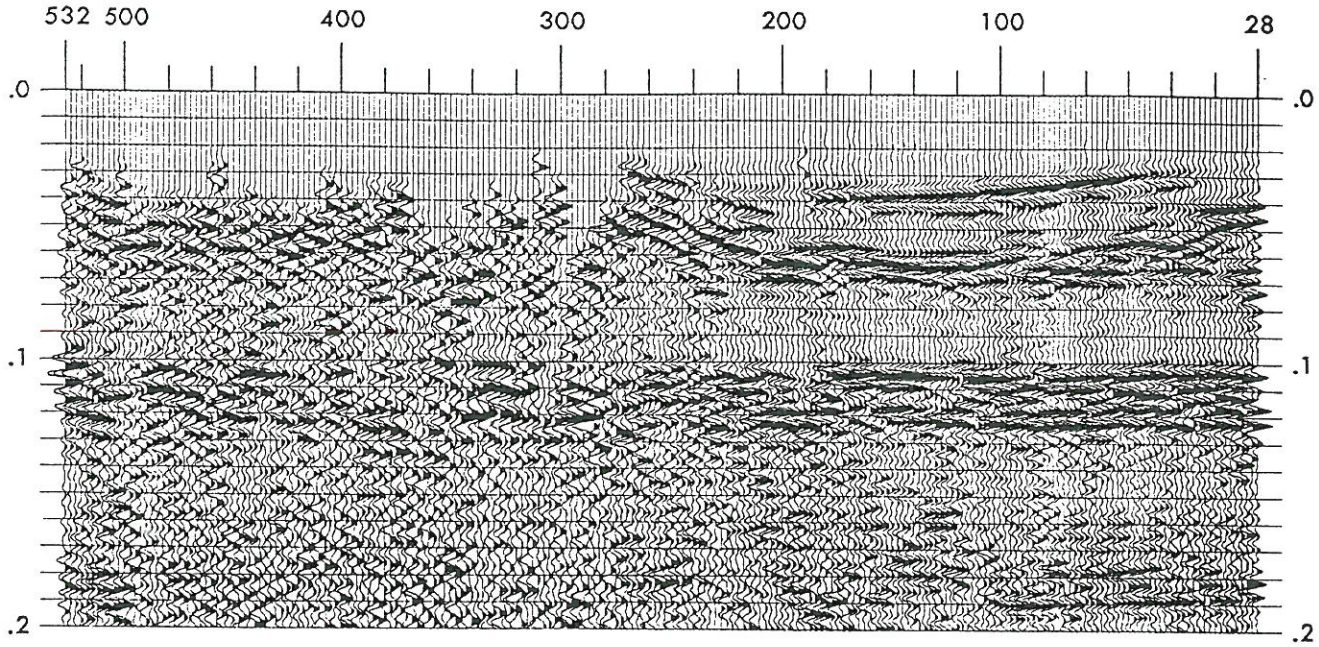

Fig. 2.4 Reflection seismic profile from the Nr. Lyngby locality acquired in 1986.

In order to make a more detailed investigation of this phenomenon a high resolution seismic profile were acquired with significantly denser source and receiver spacing than used in previous survey. The acquisition and the processing of this profile will be described in the following section.

Acquisition

The reflection seismic profile was acquired in June 1993. The recordings were made at shot point intervals of 4.0 m and with a geophone spacing of 2.0 m. End-on recordings with a minimum offset of 2.0 m and a spread length of 52.0 m were used. The recordings were made on a 26 channel recording unit (Geometrics ES-2420) with single 14 Hz vertical component geophones. Thus, with the present recording geometry a nominal fold of 6 was achieved.

As seismic source very small charges of 2 g were used, which were placed 2.0 m below the surface in holes drilled by a small hydraulic driven auger bit. The charges applied are made by compressed powder and, as the following examples will demonstrate, has produced very high frequency reflections, on the assumption that optimal conditions for the acquisition are present. The position of the reflection profiles is shown in Fig. 2.5. The relative position of the wells, on which part of the geological description and the geotechnical tests are based, are also indicated.

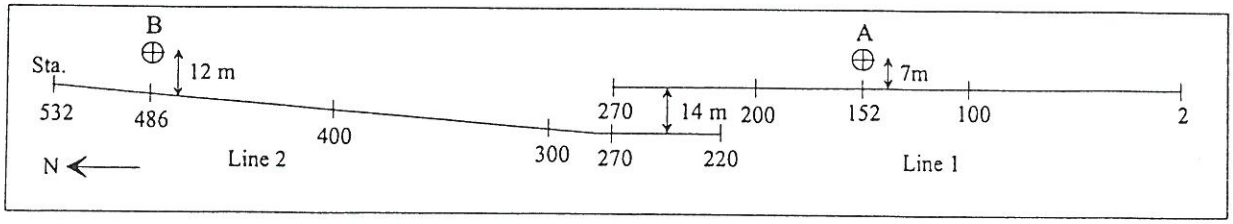

Fig. 2.5. The position of the reflection seismic profiles relative to the wells.

Processing

A traditional processing sequence has been applied to the reflection seismic profiles. Since the reflections observed on line 1 are of much higher frequencies than the ground roll, it is possible to recover reflections in the time-offset ranges where surface waves dominate. Therefore, a low-cut filter as high as 200 Hz is used. Although data are acquired at almost exactly the same elevation, automatic static corrections gave some improvement of the data quality, which must be assigned to local near-surface velocity variations and the fact that high frequency reflections are present. The static corrections are made by stack-power maximization (Ronen, 1985) and (Nørmark, 1993). The processed line 1 is given in Fig. 2.6. Reflections have been observed to the end of the data at 700 ms, but only the uppermost 200 ms are shown. The migrated section from line 1 is given in Fig. 2.7. The migration has particularly improved the horizon at about 60 ms two-way traveltime.

Along line 2 a remarkable change in data quality is observed, which is mainly characterized by a shift to significantly lower frequencies. Consequently, ground roll and reflections could not be separated by frequency filtering in this area. Instead a tail mute has been applied in order to remove the high amplitude surface waves. Otherwise, the same kind of data processing has been used as on line 1, except for a low-cut filter of 50 Hz. The stacked unmigrated data from line 2 are shown in Fig. 2.8.

Spectral content of signals generated by shots with different charge size

The data acquired by 2 g and 25 g of dynamite have already indicated that the charge size has a significant impact on the spectral content and thereby on how the reflections are attenuated. In order to make a comparison to conventional seismic data and to the charge sizes normally used in such surveys, additional shots with 500 g dynamite have been recorded. These shot gathers are shown in Fig. 2.9 together with shot gathers from approximately the same position acquired by 2 g charges. The surface waves appear in different time-offest ranges on the 500 g shots than on the 2 g shots since the former recordings are made at larger offsets. As expected the shot gathers acquired by 500 g charges are not as sensitive to variations of the surface layers as the shot gathers acquired by use smaller charge sizes. This is also evident on the amplitude spectra from selected traces between 80 ms and 140 ms which is shown in Fig. 2.10.

By comparing the amplitude spectra for different charge sizes in the southern part of the survey area at Sta. 220 it is evident that much lower frequencies are generated by using bigger charge sizes. For the 500 g shots peak frequencies between 80 Hz and 150 Hz are observed, whereas a much wider spectra, with peak frequencies between 200 Hz and 400 Hz, have been obtained on the 2 g shots. By making a similar comparison in the northern part of the survey area at sta. 480 the most low-frequent data are here surprisingly observed for the 2 g shots. The reason for this is presumably that the low amplitude and high frequency signals generated by the 2 g shots have been attenuated so much that only signals at the lowest frequencies remain.

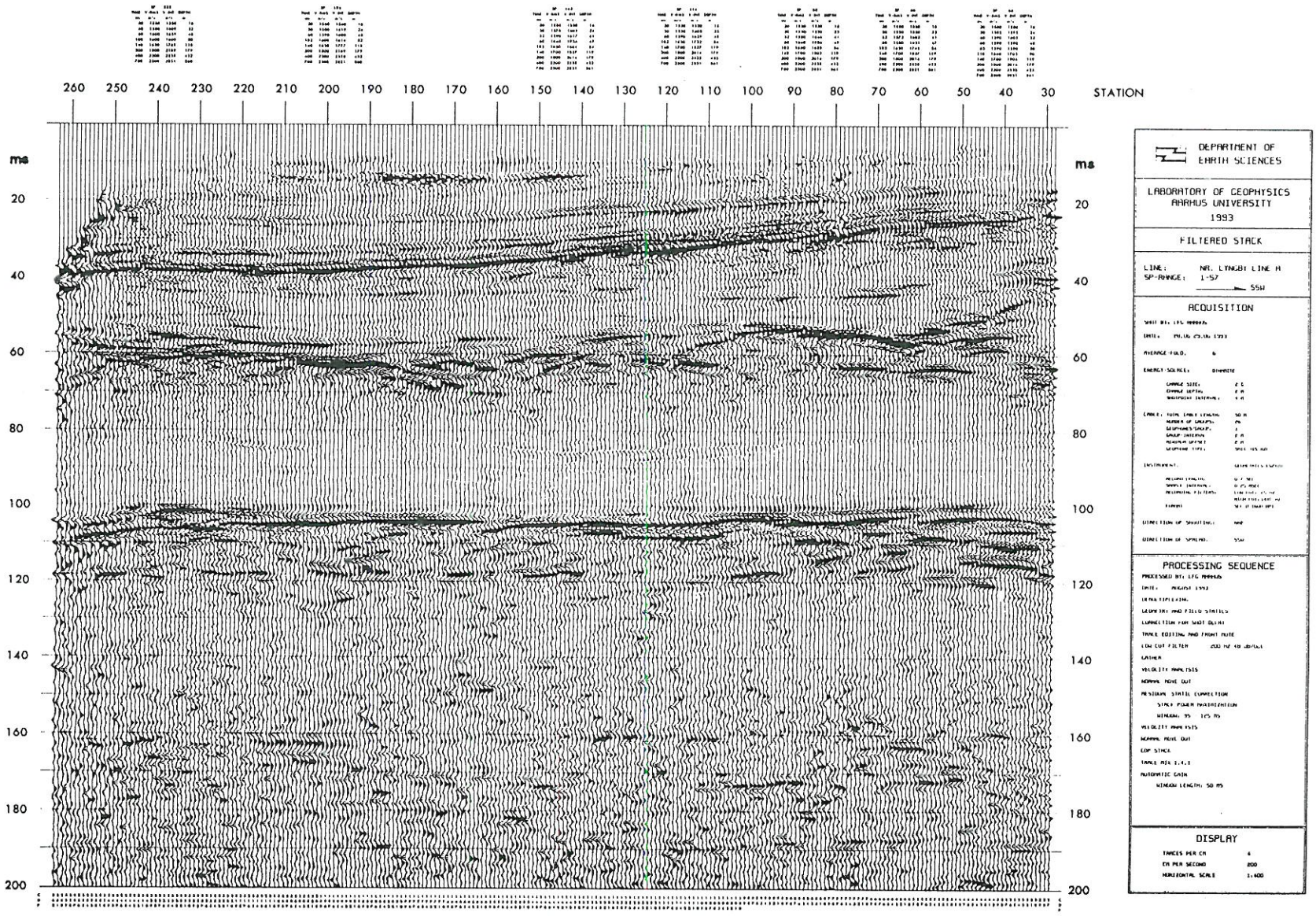

Fig. 2.6 Unmigrated section from line 1.

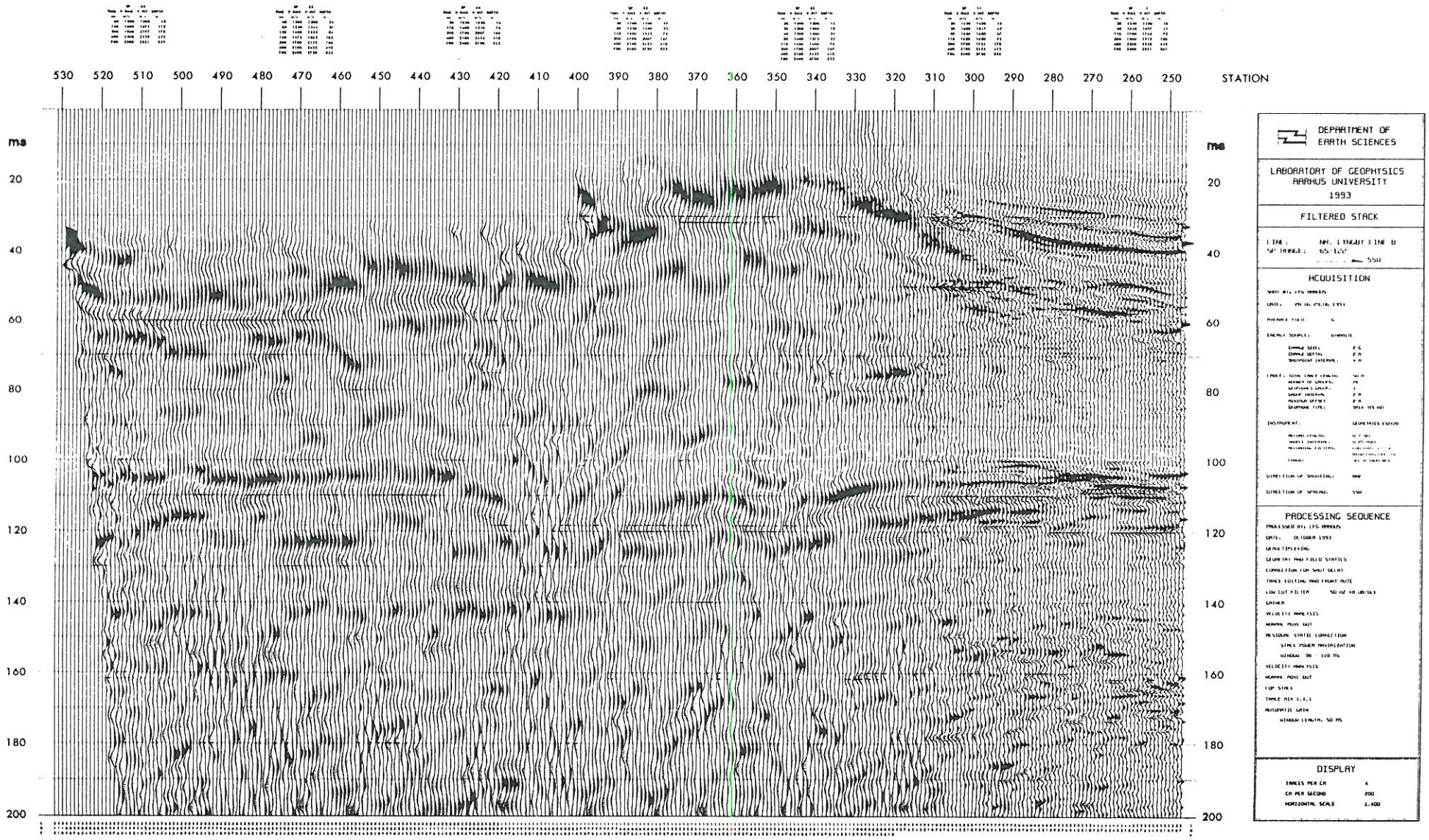

Fig. 2.8 Unmigrated section from line 2.

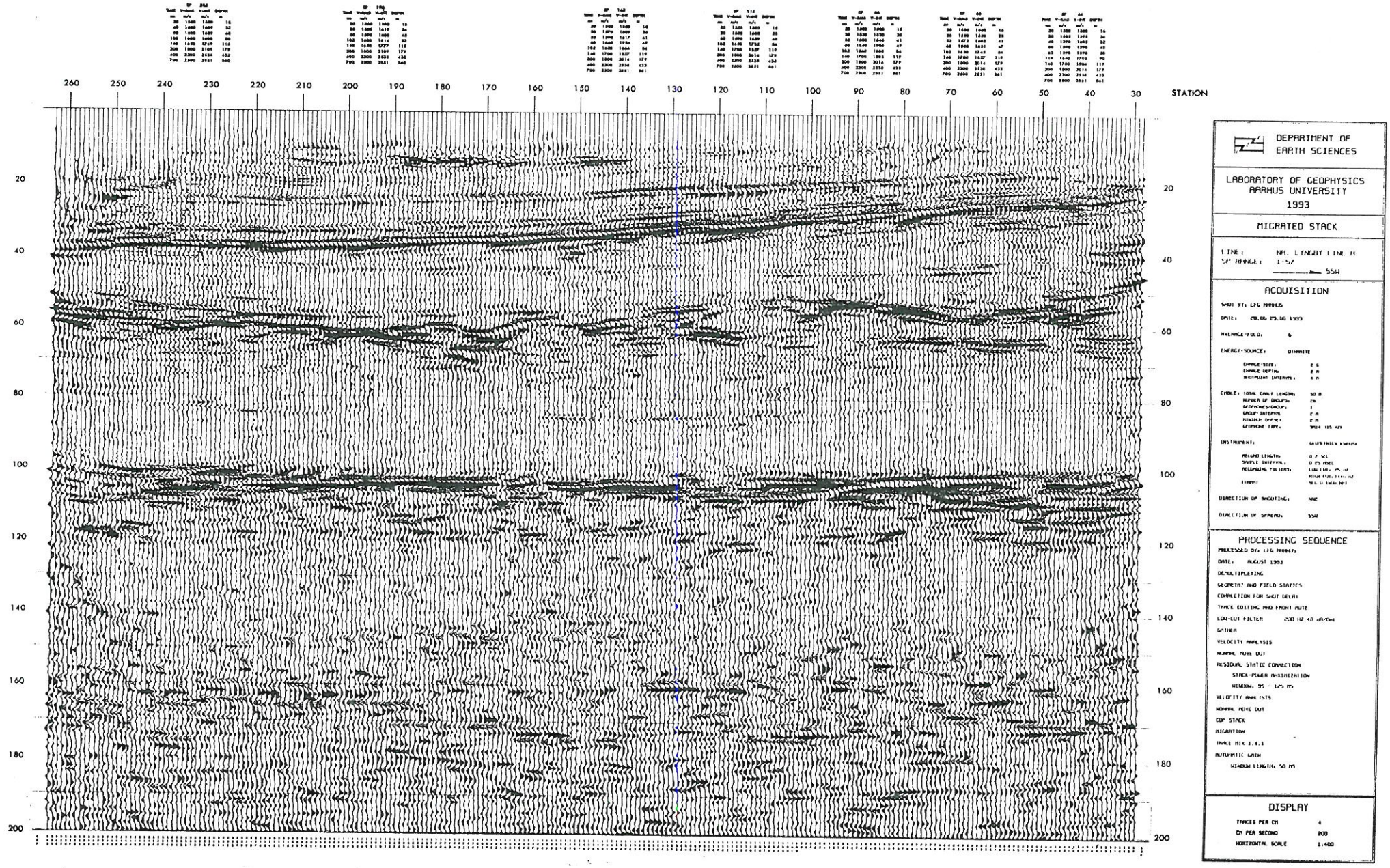

Fig. 2.7 Migrated data from line 1.

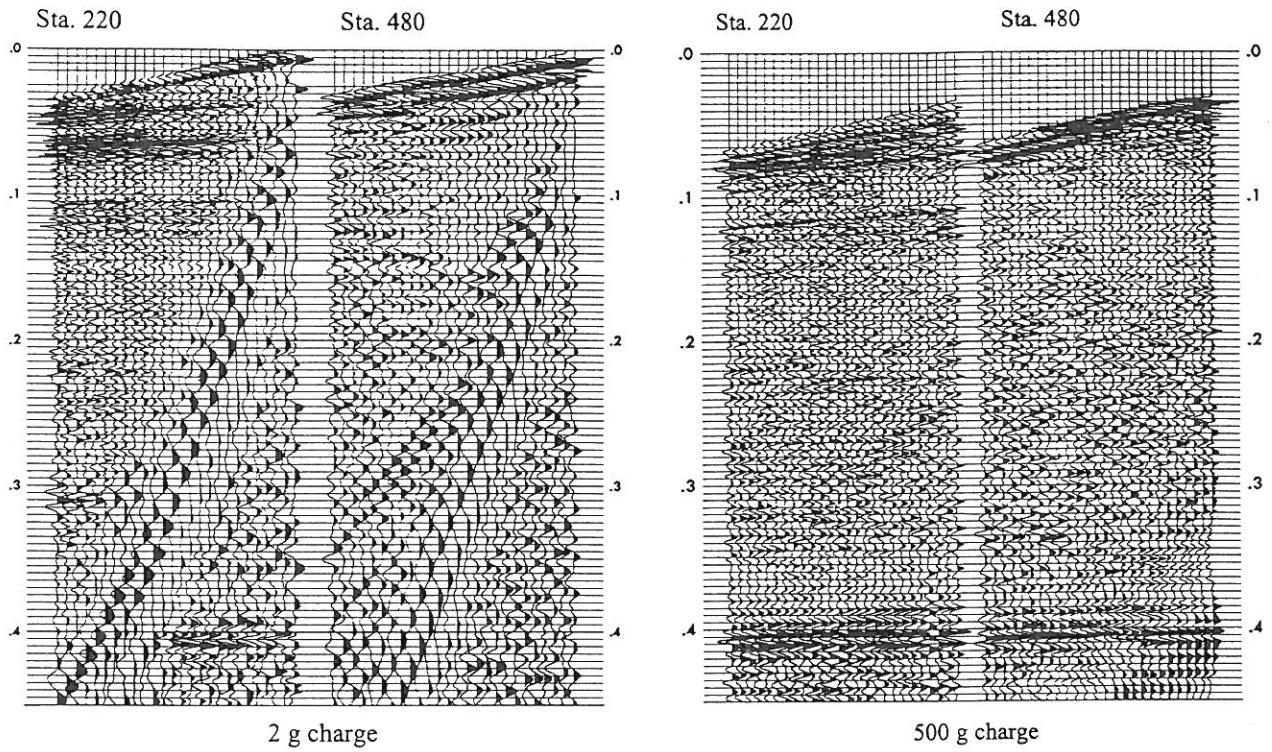

Fig. 2.9 Shot gathers acquired by use of by 2 g and 500 g of dynamite.

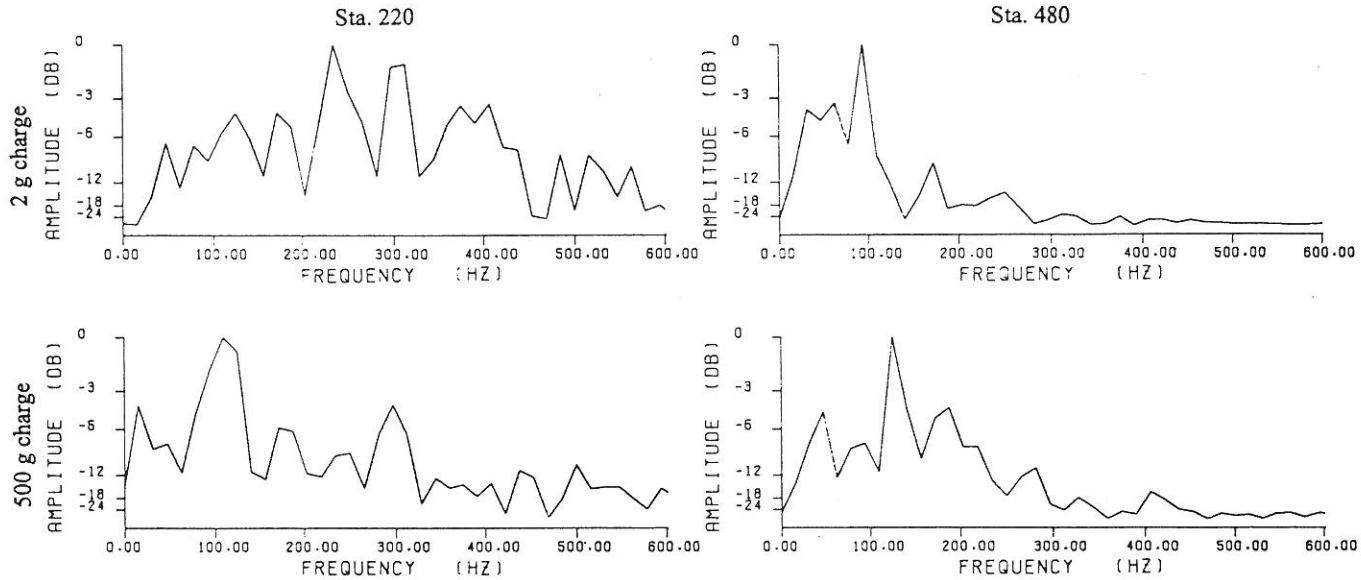

Fig. 2.10 Amplitude spectra of selected traces from the shot gathers in Fig. 2.9.

The present qualitative comparison indicates, like the data from the southern part of Jutland, that shallow seismic data are much more sensitive to variations in the near surface layers than conventional seismic data. However, in the present examples potential variations in the source signals cannot be distinguished from attenuation effects. Yet, on the present locality there is good opportunity to eliminate the effects from such variations by acquiring data across the transition zone, which on the stacked section appear to be in the interval from Sta. 320 to Sta. 360.

The transition zone between regions with different acoustic properties

By acquiring data across the interval with different acoustic properties it is possible to shoot in the material where high frequency signals are generated, into the area with high attenuation. Thereby, the potential variations of the source signals from one kind of sediment to another are eliminated. Four different charge sizes are used: Cap detonator (C.D.), 8 g compressed powder, 25 g and 100 g dynamite with shot points close to each other. The shot gathers are shown in Fig. 2.11. The receivers are placed at the same position. It should be noted that the very significant variations in the spectral content of the reflected data take place over less than 2.0 m for all charge sizes. In Fig. 2.12 the amplitude spectra for traces indicated in Fig. 2.11 which are only 2 m apart are shown. The same scaling has been applied on the amplitude spectra such that comparison between different shots and different traces is possible.

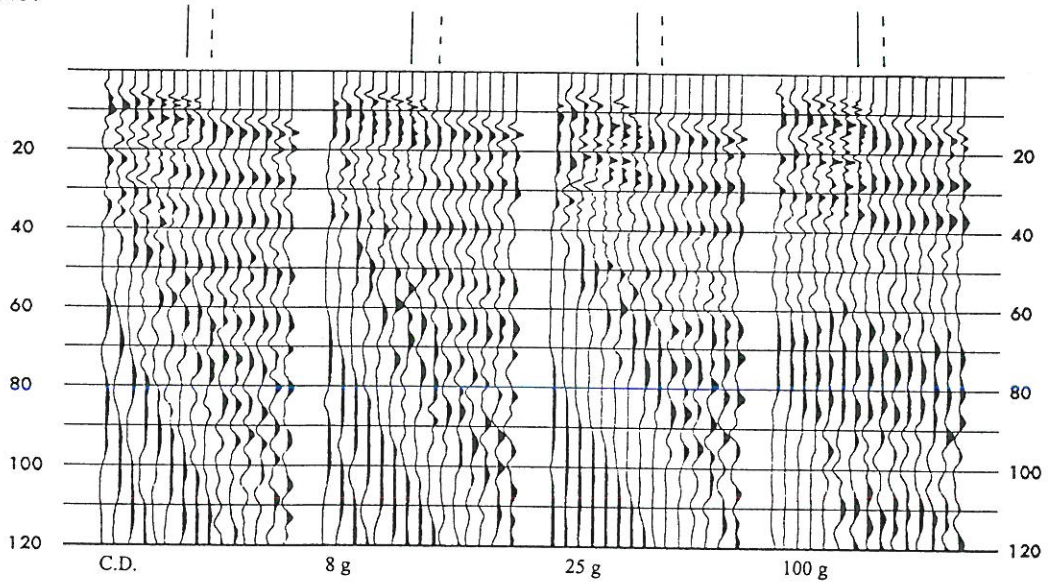

Fig. 2.11 Selected traces from shot gathers acquired across the transition zone with different charge size. The receiver spacing is 1.0 m.

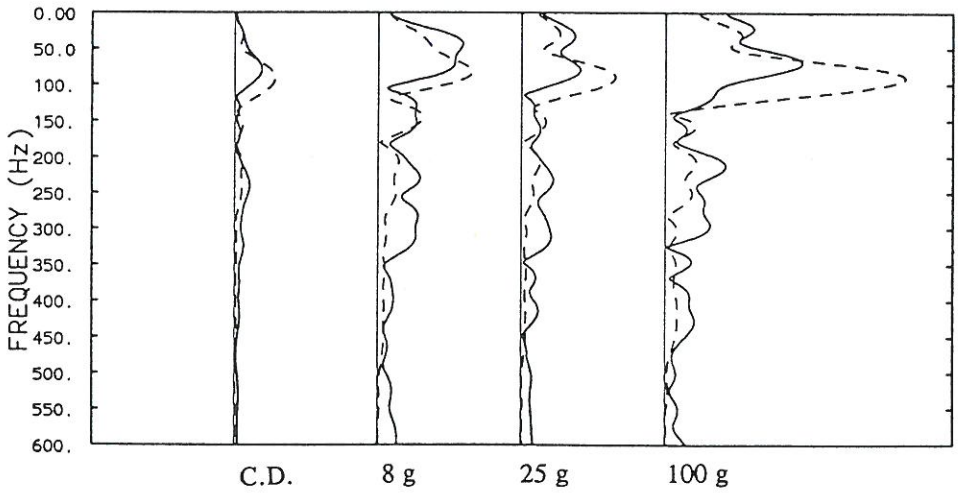

Fig. 2.12 Amplitude spectra for shallow reflection for traces indicated in Fig. 2.11.

It is observed that the most wide spectra has been obtained for 8 g and 25 g shots. Otherwise, the same development in the amplitude spectra are observed for all charge sizes. Above 120 Hz the data are as expected attenuated at increasing offsets. However, for unknown reasons it seems that energy are not attenuated as much as expected below 120 Hz in the area with poorer acoustic properties. This is apparent on all shot gathers but most pronounced on the 100 g shots. The present shot gathers demonstrate that properties for the wave propagation are of main significance for the appearance of seismic data at this place. In section 7 synthetic seismic data are simulated across the transition zone for estimating the attenuation for signals above 120 Hz.

3 Geological description of the Nr. Lyngby locality

Nr. Lyngby is situated in the NW-SE trending transition zone between the Fennoscandian Shield and the North Sea Basin (Fig. 3.1). This so-called Sorgenfrei-Tornquist Zone is characterized by relatively strong tectonic activity. The most recent tectonic activity was in the period Late Cretaceous-Early Tertiary where the zone acted as a zone of wrenching due to compression from southerly directions. During this episode inversion structures were formed (Liboriussen et al., 1987).

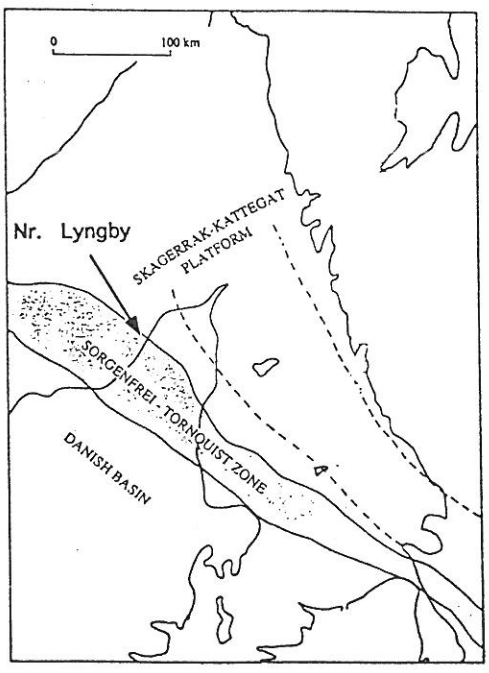

Fig. 3.1. Nr. Lyngby is located in the Sorgenfrei-Tornquist Zone between the Skagerrak-Kattegat Platform fringing the Fennoscandian Shield and the North Sea Basin.

The shallow (i.e. to depths around 500 m) geology at Nr. Lyngby is relatively simple and well documented by wells and seismic investigations. The large-scale stratigraphic and lithological features are documented by the well DGU 8.21 as summarized in Fig. 3.2. This well is located about 1 km south of Nr. Lyngby (Fig. 3.3). An about 120 m thick series of Quaternary beds rest on the eroded surface of Upper Cretaceous white chalk and limestone. Below the 350 m thick chalk/limestone sequence a clayey sequence of early Late Cretaceous and Early Cretaceous age are encountered. The transitions at the top and the base of the chalk/limestone sequence form excellent seismic reflectors.

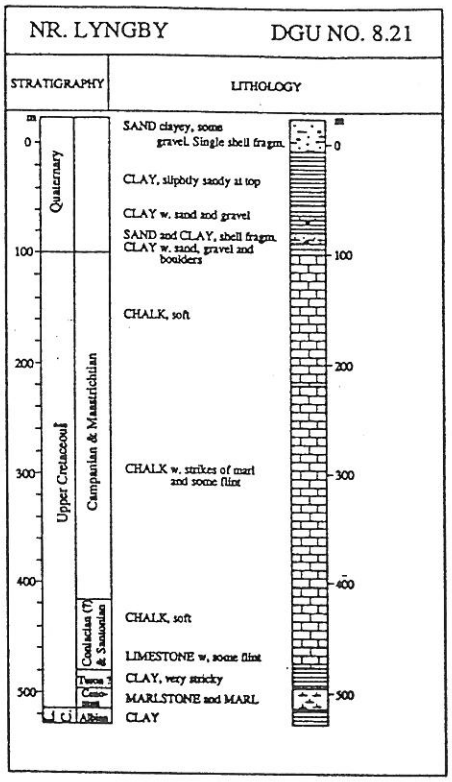

Fig. 3.2. Stratigraphy and lithology of the well DGU 8.21. For location see Fig. 3.3.

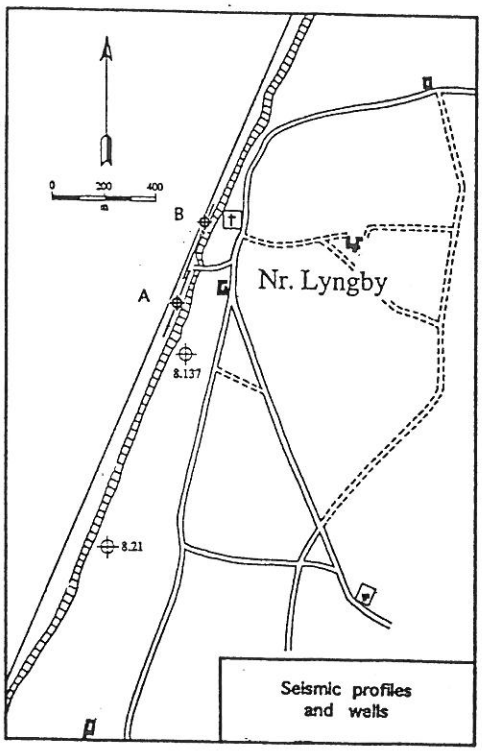

Fig. 3.3. Location of wells in the vicinity of Nr. Lyngby.

The Quaternary sequence has been described in some detail in a well (DGU 8.137) located about 0.5 km south of Nr. Lyngby (Fig. 3.3). The main lithological constituent in the Quaternary is clay with varying content of silt and sand (Fig. 3.4). Few intervals dominated by sand are found in the upper part of the sequence above sea level. Based on their content of foraminifera and molluscs the layers penetrated are all considered to of marine origin and ranging in age from Late Saalian to Late Weichselian (Lykke-Andersen, 1987).

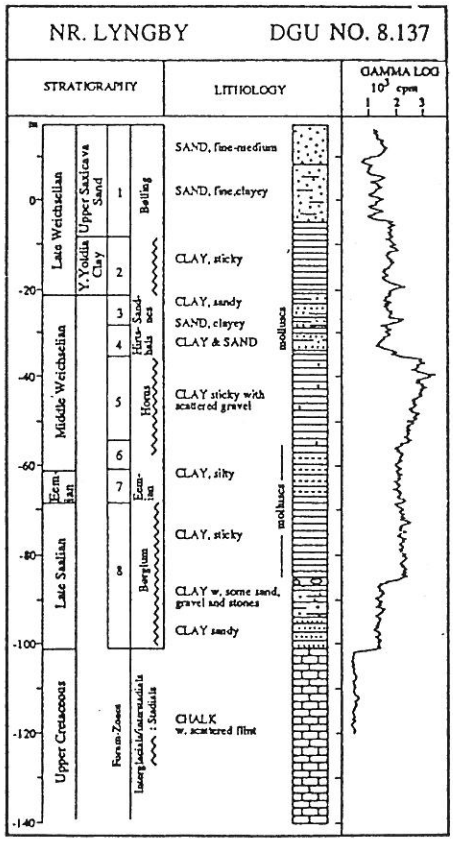

Fig. 3.4. Stratigraphy and lithology of the well DGU 8.137. For location see Fig. 3.3.

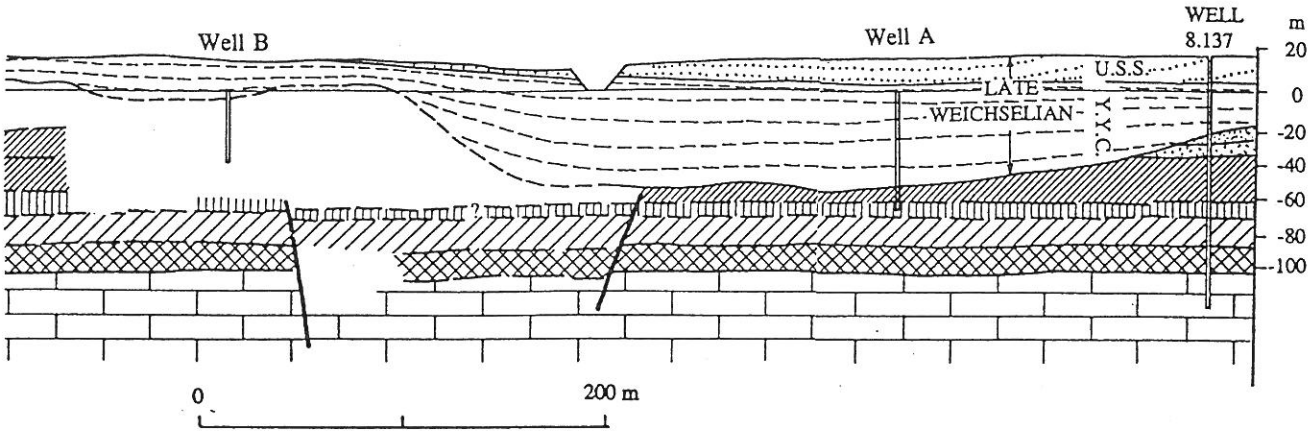

Fig. 3.5. Geological cross section at Nr. Lyngby based on reflection seismic profiles and wells.

Based on data from the two wells and high resolution reflection seismic profiles acquired along the beach a geological cross section was constructed as shown in Fig. 3.5.

The architecture is quite simple: Late Saalian- Middle Weichselian deposits form a layer-cake with approximately horizontal layers resting on the almost horizontal surface of the Upper Cretaceous chalk. This layer-cake is cut by an about 1000 m wide erosional channel reaching levels of about 50 m b.s.l. The erosional channel is filled by Late Weichselian deposits consisting of a lower clay sequence and an upper sandy sequence, the latter mainly restricted to levels above sea level.

The layer-cake sequence seems to be affected by small-scale faulting as indicated on Fig. 3.5. The faults below the northern flank of the erosional channel are speculative due to the fact that the resolution in the seismic profiles deteriorates at this place. The offsets on the faults below the southern flank of the channel are few metres.

Gas in the Quaternary sediments in Northern Jutland

The occurrence of methane gas in the Quaternary deposits is well known in the northernmost parts of Jutland. Early investigations (Jessen et al., 1910) showed that methane gas of biogenic origin (i.e. gas formed by decay of organic matter contained in the Quaternary sediments) is present in several levels in the Quaternary sequences. The occurrences are mainly restricted to the northeastern part of Vendsyssel (Jessen, 1936) and seem to be delimited by the northeast flank of the inverted Sorgenfrei-Tornquist Zone (Fig. 3.6).

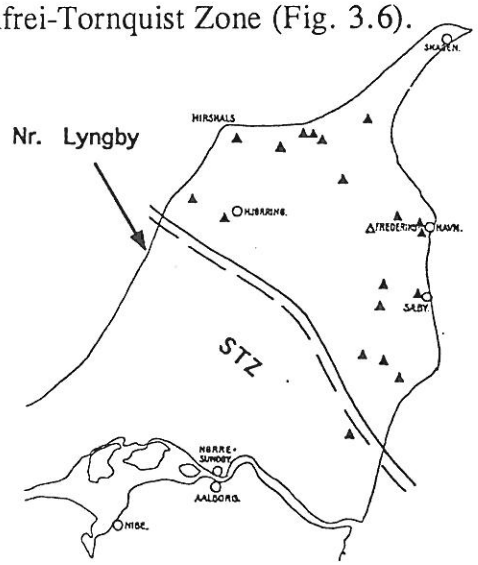

Fig. 3.6. Distribution of biogenic methane gas in Quaternary deposits in Vendsyssel.

New wells at Nr. Lyngby

The two cored wells that was carried out in order to investigate the mechanical properties of the shallow Quaternary sediments was analyzed lithologically and stratigraphically.

Sediments were described by visual inspection of one half of the split cores. Grain size distributions were performed by sieving fractions larger than 125 microns and by analyzing the finer fraction by means of a "Sedigraph". Results of the grain size analysis are shown in Figs. 3.7 and 3.8 together with the lithological descriptions.

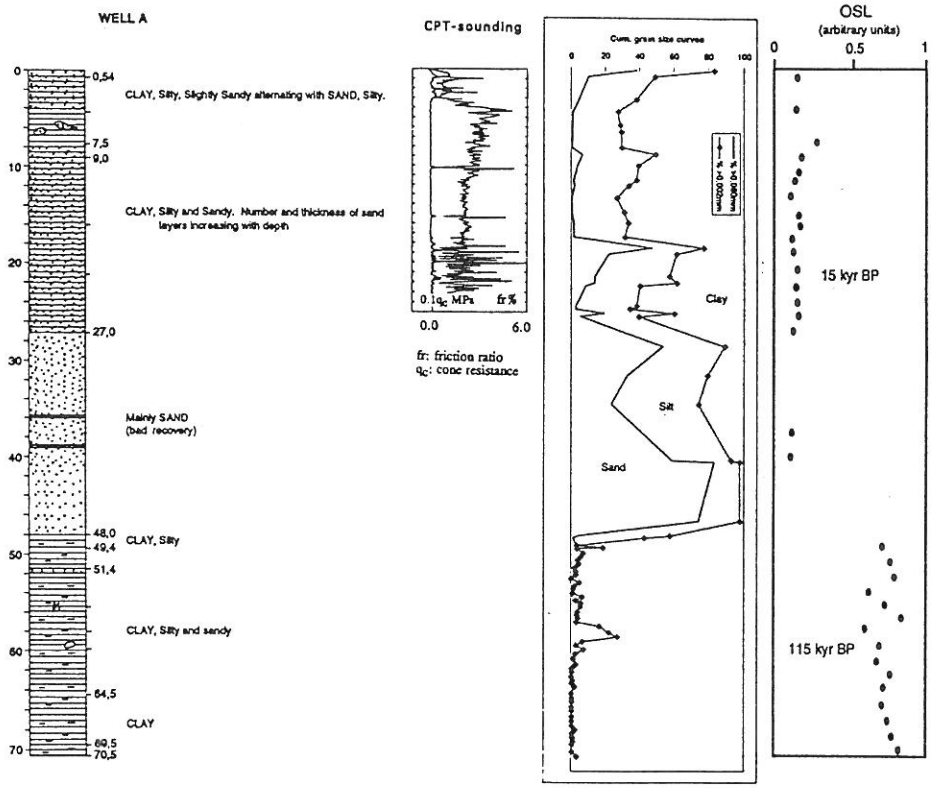

Fig. 3.7. Well A: Lithology and stratigraphy.

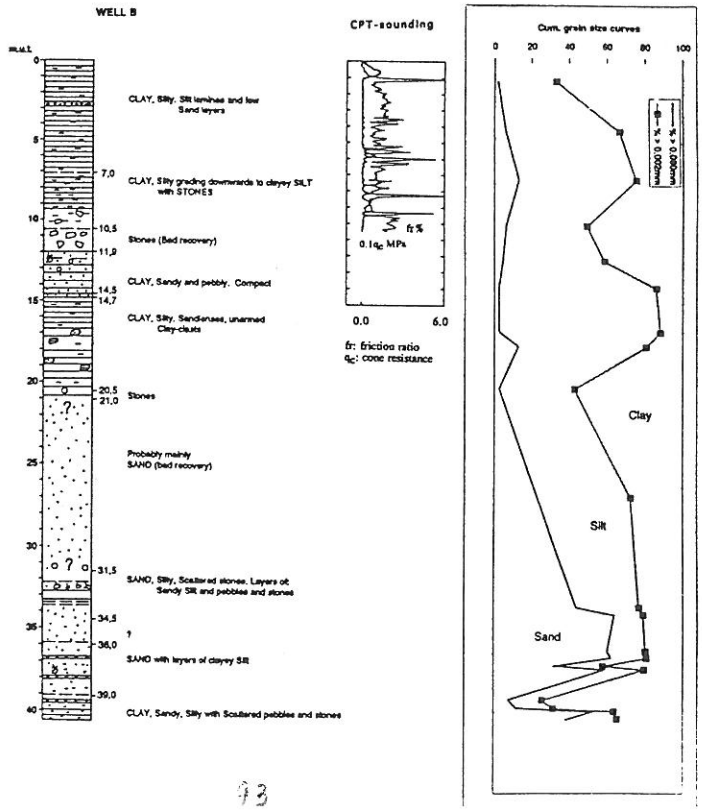

Fig. 3.8. Well B: Lithology and stratigraphy.

4 Laboratory work

General

The purpose of the laboratory testing of material from the actual site was to determine the dynamic properties of the soil. The planned testing was to classify the soil by well known classification tests and to determine the overconsolidation ratio and the deformation parameter from oedometer tests. On the basis of these results a test program was set up to determine the dynamic parameters of the soil. Resonant column tests were carried out at different amplitudes and frequencies to determine the elastic parameters, E (Young's modulus) and the amplification or damping factor, D. The S-wave velocity, v_s, and the shear modulus, G was determined by the bender element method. The laboratory tests were carried out on undisturbed samples, and the results are compared to the results obtained by the seismic investigations at the actual site.

Samples for laboratory testing

The undisturbed samples for laboratory testing were extracted using a thin-walled sampler, 72 mm in diameter. Undisturbed samples were extracted from the clayey sediments in boring A and B and 10 undisturbed samples have been extracted from the clayey sediments in 2 m's depth below the surface along the seismic line. For resonant column tests only undisturbed samples were used. Some parts of the cores from boring A and B were sealed immediately after the coring and some of these cores were used for classification tests and oedometer tests. From 2 m's depth below surface along the seismic line, 4 samples for classification tests were extracted with a thin-walled sampler, 42 mm in diameter. All the samples were stored at a temperature of + 5 ° C until the tests were carried out.

Classification tests

The soils are classified by determination of

1) w - water content = weight of water in per cent of dry weight
2) Atterberg limits and plasticity index
   - w_L - water content at the liquid limit (limit between liquid and plastic stage)
   - w_P - water content at the plastic limit (limit between plastic and semi solid stage)
   - I_P - plasticity index = $w_L - w_P$
3) k_a - lime content - weight of $CaCO_3$ in per cent of dry weight
4) gl - loss on ignition in per cent of dry weight
5) γ - unit weight.

The results of the classification tests are shown in fig. 4.1 and fig. 4.2. The results of the classification tests do not show any significant variations along the seismic line from the south to the north.

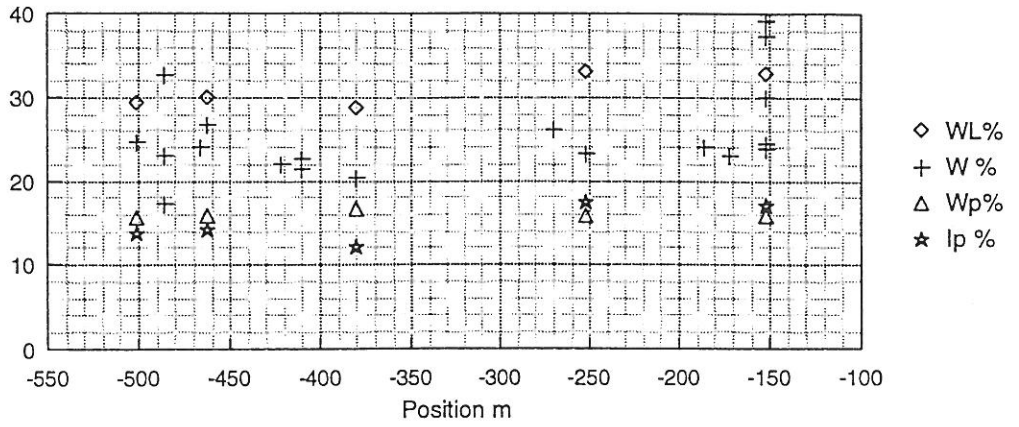

Fig. 4.1 Water content, Atterberg limits and plasticity index plotted along the seismic line.

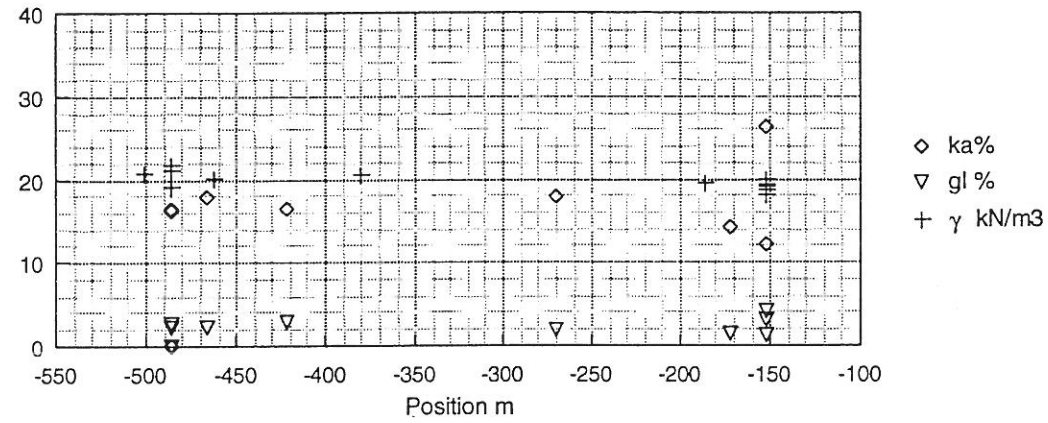

Fig. 4.2 Lime content, loss on ignition and unit weight plotted along the seismic line

Oedometer tests

The actual oedometer tests were carried out in the Danish Oedometer Test Apparatus, which has a floating ring (Moust Jacobsen, 1967). The registration of the deformations during the tests has been automatic and continuous using transducers with an accuracy of 10^{-3} mm.

In an oedometer test the sample is subjected to a stepwise increase in the effective stress. Each new load on the sample produces an increase in the vertical total stress and an excess water pressure is built up in the voids. During the consolidation process, which is drainage of the excess porewater pressure, the effective stress increases. The consolidation process is followed for each load step by continuous observations of connected values of deformation and time. An oedometer test provides information about the following values (Thorsen, 1995):

1) σ'_{pc}- the preconsolidation pressure = the largest effective stress, the material has ever been subjected to. When the effective stress in situ, $\sigma'_{0,}$ is known, the over consolidation ratio, OCR, can be determined (fig. 4.3).

2) $Q = C_c/(1+e_o)$, where C_c is the coefficient of compressibility and e_o is the initial void ratio. The effective stress, σ', plotted against the consolidation strain, ε_c, shows a rectilinear variation of ε_c with log σ' for σ' larger than the preconsolidation pressure, $d\varepsilon_c = Q \, d\log \sigma'$. (fig. 4.3).

3) Q_s- Creep index. Each time-settlement curve contains consolidation settlements as well as creep settlements. The creep settlements have shown to vary rectilinear to log time after a certain period, $d\varepsilon_{cr} = Q_s \, d\log t$. (fig. 4.4).

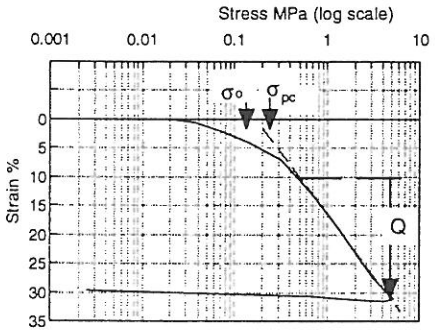

Fig. 4.3 Oedometer test. Strain, ε_c, against effective stress, σ'

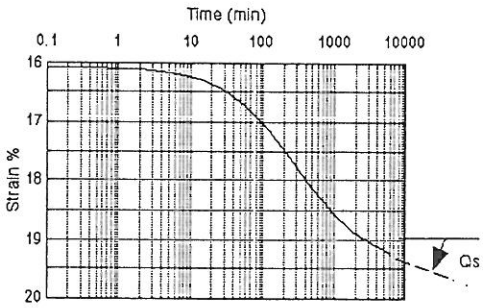

Fig. 4.4 Oedometer test. Time settlement curve for $\sigma' > \sigma'_{pc}$

Oedometer tests have been carried out with 5 samples from cores extracted from boring A and B, and with two undisturbed samples extracted from 2 m below surface in the seismic line station 186 and 462.

Determination of the preconsolidation pressure, σ_{pc}' and the parameters for deformation, creep and swelling. Q and Q_s, is important to plan the test conditions for the resonant column tests, since the dynamic parameters of the soil are very sensitive to changes in the void ratio. All the test results indicate an OCR > 2. In order to reestablish the in situ conditions after sampling, the samples are consolidated at an effective pressure between the in situ pressure, σ_0', and the preconsolidation pressure, σ_{pc}', and then unloaded and consolidated at σ_0', before the dynamic tests are carried out. Determined values for Q and Q_s, are shown in fig. 4.5

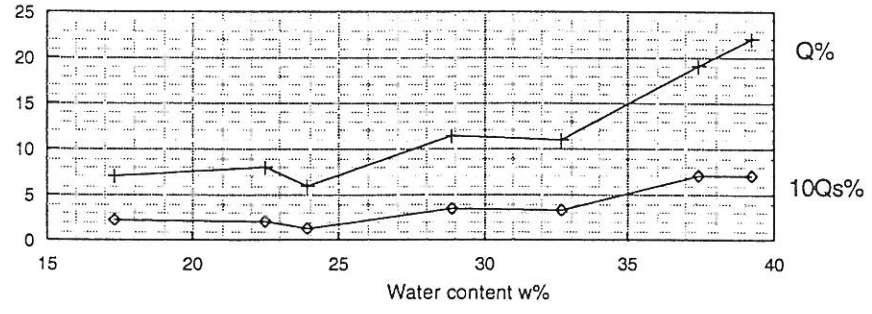

Fig. 4.5 Results from oedometer tests.

Resonant column tests and tests with bender elements

General

Two different test procedures have been performed in the laboratory to determine the dynamic parameters of undisturbed samples of Yoldia clay from the actual area at Nr. Lyngby.

1) Longitudinal resonant column test, which is performed to determine Young's modulus, E, and the material damping ratio, $D = E_v /(4\pi E_e)$, where E_v is the energy, which disappear per cycle and E_e is the energy used for the elastic compression under a steady state condition.

2) Test with bender elements, which is performed to determine the shear modulus, G.

The test-setup

The test-setup for the longitudinal resonant column device fitted with bender elements to facilitate determination of the shear modulus is sketched in fig. 4.6.

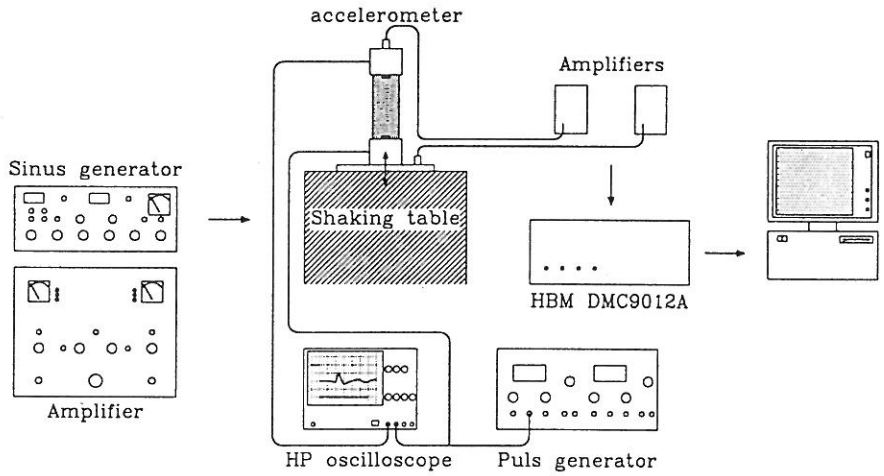

Fig. 4.6 Longitudinal resonant column device fitted with bender elements in the top cap and base cap.

The longitudinal resonant column method consists in applying a sinusoidal axial displacement to the soil specimen. The applied displacement generates rod compression waves that travel through the specimen. Measuring the acceleration at the top and bottom of the specimen facilitates determination of the natural frequency, f_n. By varying the frequency of the applied displacement, the variation of the amplification factor, H, with frequency is determined. The amplification factor is defined as the ratio between the acceleration at the top and the acceleration at the bottom of the specimen. The natural frequency is defined as the frequency at which the amplification factor shows a maximum. On the basis of the natural circular frequency, ω, the amplification factor, H, the height, h, and the density, ρ, are the following values calculated (Moust Jacobsen, 1990):

1) Young's modulus, $E = \rho(\omega h/\alpha)^2$, where α is a factor depending of the oscillating mass (the mass of the specimen and the upper cap)

2) The material damping ratio $D = 1/(2H)$

The S-wave velocity is determined by means of bender elements placed at each end of the soil specimen (Dyvik and Madshus, 1985). Bender elements are piezoceramic elements, where one element is used to generate a S-wave which propagates along the length of the specimen, and the other element is used as a receiver of the S-wave. In this way the travel time of the S-wave is determined. On the basis of the travel time, t, the travel length, l, and the density, ρ, are the following values calculated:

1) the S-wave velocity $v_s = l/t$

2) the shear modulus $G = \rho(v_s)^2$

The maximum shear strain level determined near the transmitter element is estimated to approximately 10^{-3} %, (Dyvik and Madshus, 1985).

Test procedure

The undisturbed samples were carefully extracted from the tubes and shaped to fit the resonant column apparatus. The shaped specimens were encapsulated in latex membranes and by a vacuum system subjected to a "preconsolidation" pressure at 1.1 to 1.5 times the effective in situ pressure, σ_0', or to 90 kPa for the samples with an effective in situ pressure of more than the vacuum pressure. The soil is consolidated at a pressure between σ_0' and σ_{pc}', in order to restore the natural conditions after sampling. Drainage in the tests were performed as radial drainage by means of filter strips placed around the specimen.

After consolidation at the "preconsolidation" pressure, the samples were consolidated at an all round pressure as close as possible to the in situ pressure. After consolidation at the in situ pressure the S-wave velocity was determined by means of the bender elements, followed by a test to determine Young's modulus carried out on the same specimen at the same stress conditions. A new test was carried out with the bender elements, to see if the soil material had changed during the longitudinal resonant column test.

After the above described procedure, the applied pressure was changed and new measurements were made after consolidation. The procedure has been repeated for each specimen for several stress levels in the range of 10 - 90 kPa.

Additional tests

Bender elements have also been fitted into the caps used in the Danish Triaxial Cell to facilitate determination of the S-wave velocity at higher stress levels. Mounting the elements in the caps in the triaxial cell facilitated measurements of the S-wave velocity for stress levels up to 400 kPa. Two tests were carried out in this apparatus at stress levels up to 400 kPa. For one test measurements were carried out for both OCR = 1 and OCR = 1.5, but no significant difference in the results were registered.

Test results

A total of 9 resonant column tests have been performed as well as two additional tests in the triaxial apparatus. The major part of the tests have been performed on samples extracted from the clayey sediments in 2 meters depth, but 2 samples from 4.5 meters depth and 1 sample from 16 meters depth have also been tested. The results of the determination of the S-wave velocity are shown in fig. 4.7 - 4.9.

From the resonant column tests both Young's modulus and the shear modulus have been calculated. Unfortunately, it has not been possible to perform the longitudinal resonant column tests at the same low strain level as the bender element tests. The values of Young's modulus (E_{test}) from the tests are therefore not to be correlated directly.

For very small strains the Poisson ratio is very close to $\mu = 0.5$. In the bender element tests the strains are very small, and a better value for Young's modulus at very small strains (E_{calc}) may therefore be calculated on the basis of the value of the shear modulus and $\mu = 0.5$. The S-wave velocity, shear modulus, G, the measured Young's modulus, E_{test}, and the calculated Young's modulus, E_{calc}, are shown in fig. 4.7 as a function of the position on the seismic profile. The results presented are all from samples extracted from the clay sediments in the depth of 2 m below the surface, and the values correspond to test at the in situ stress.

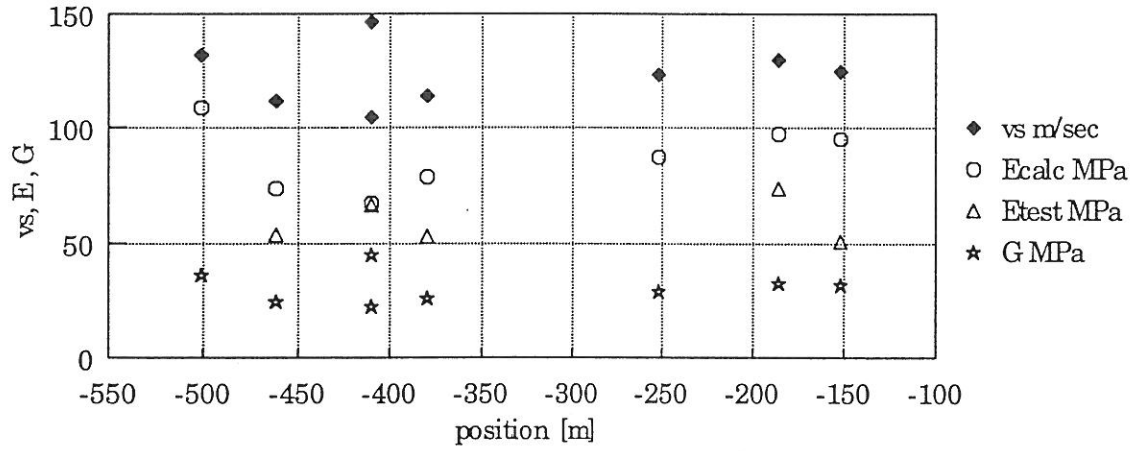

Fig. 4.7 v_s, E and G at in situ stress as a function of the position for all samples from 2m's depth.

From fig. 4.7 it is seen that there is no systematic variation in the values along the seismic profile. As expected, the calculated values of Young's modulus are higher than the measured ones.

In fig. 4.8 the S-wave velocity is plotted as a function of the stress level for all samples from 2 m's depth. The values correspond to the positions on the seismic line.

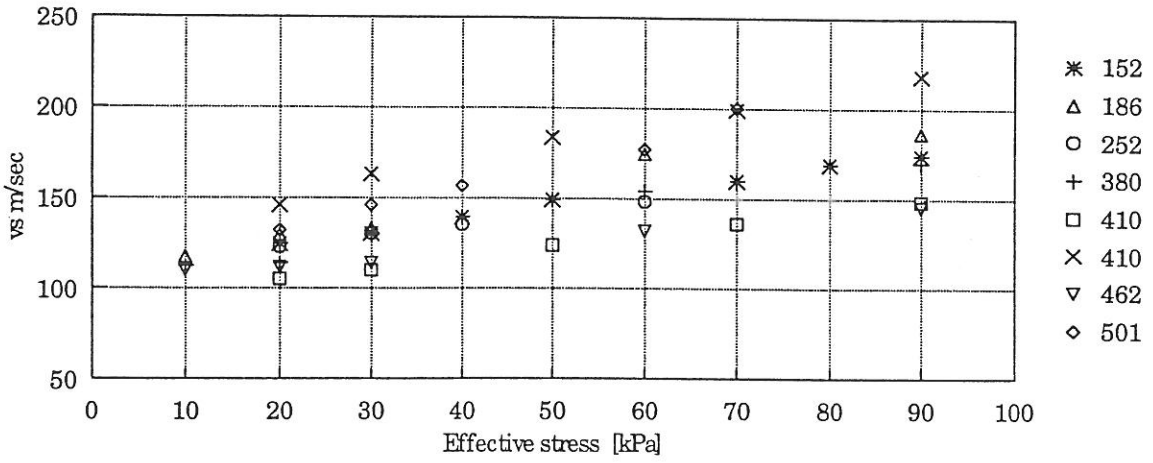

Fig. 4.8 v_s as a function of the stress level for the samples from 2m's depth.

Fig 4.8 shows that the S-wave velocity increases with increasing stress level (or density) - as expected. From the results it is not possible to state any systematic variation along the seismic profile.

In fig. 4.9 the S-wave velocity from all the tests is plotted as a function of the stress level.

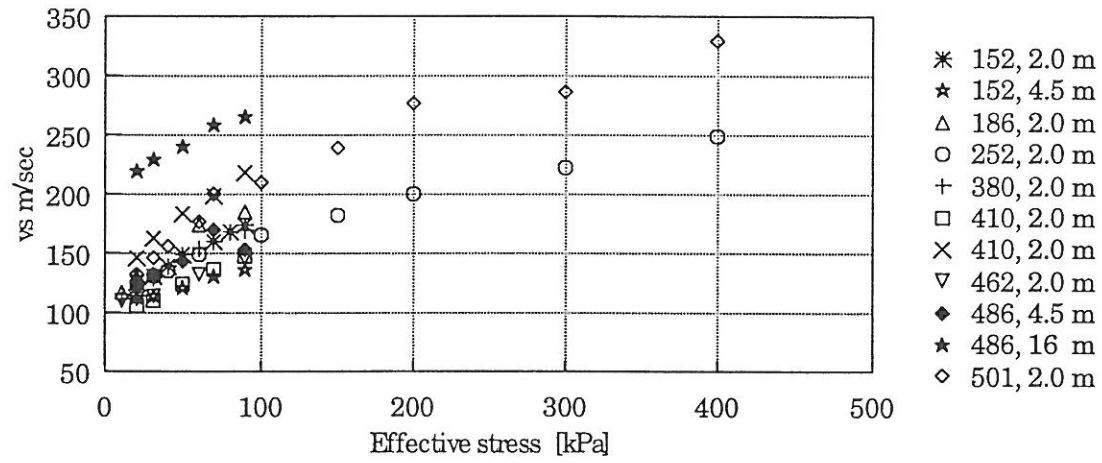

Fig. 4.9 The S-wave velocity, v_s, from all tests as a function of the stress level.

The results show that the shear velocity increases with increasing stress level (density). The sample from 16 meters depth has a void ratio (density) corresponding to the in situ pressure σ'_o~160 kPa.

In fig. 4.10 the S-wave velocity is plotted as a function of the position for different stress levels.

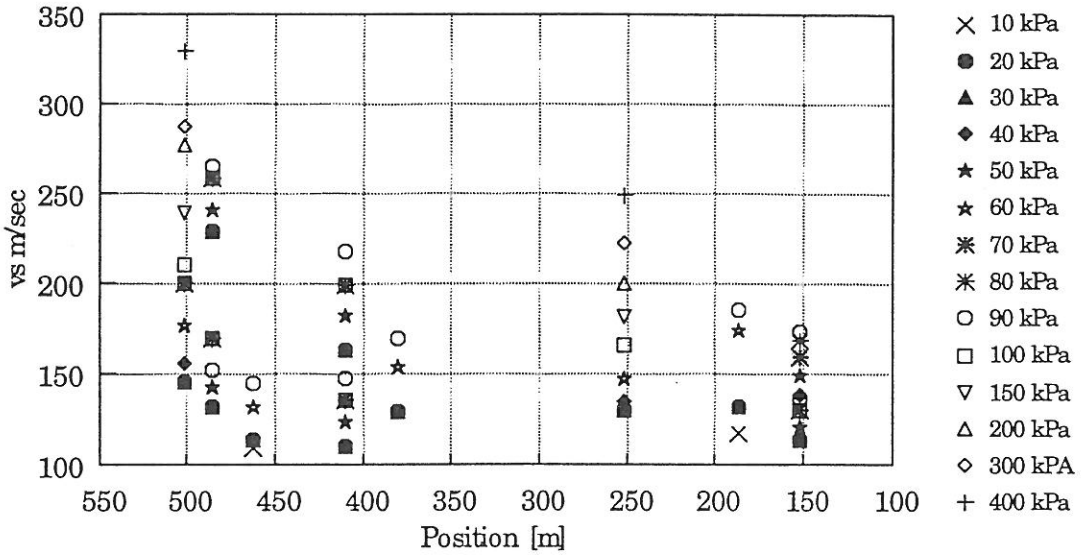

Fig. 4.10 The S-wave velocity, v_s, as a function of the position for different stress levels.

Fig. 4.9 and fig. 4.10 show that there is a tendency that for high stress levels (>100 kPa) the S-wave velocity is higher at position 500 m than at position 252 m. Only two tests have been performed at high stress levels, so it is not possible to state if the observed tendency is valid for the total seismic profile. For lower stresses, no definitive conclusions can be made.

The material damping ratio of the material, D, has also been determined from the resonant column tests. The results are plotted in fig. 4.11 as a function of the stress level and in fig. 4.12 as a function of the positions on the seismic line.

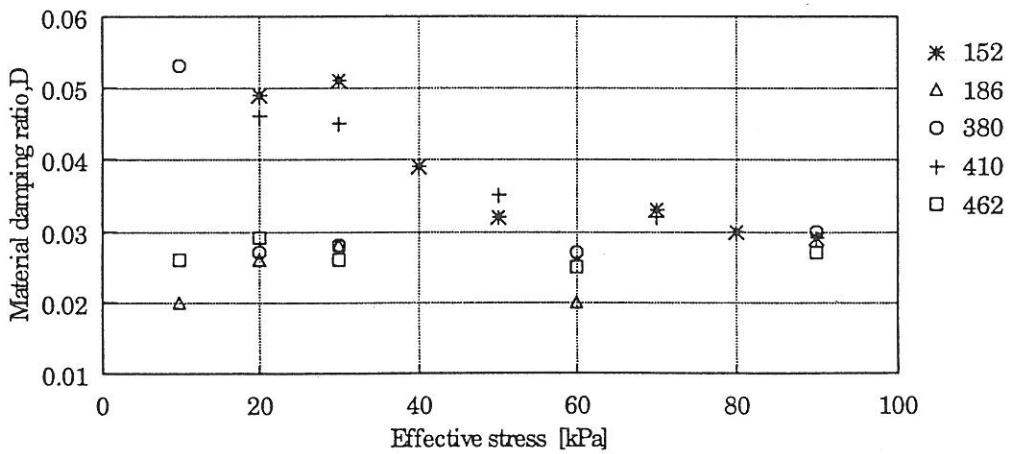

Fig. 4.11 The material damping ratio, D, as a function of the stress level.

In position 462 and 186 the damping ratio shows nearly no variation with stress level, while the results from position 152 and 410 show a decrease in the damping ratio with increasing stress level.

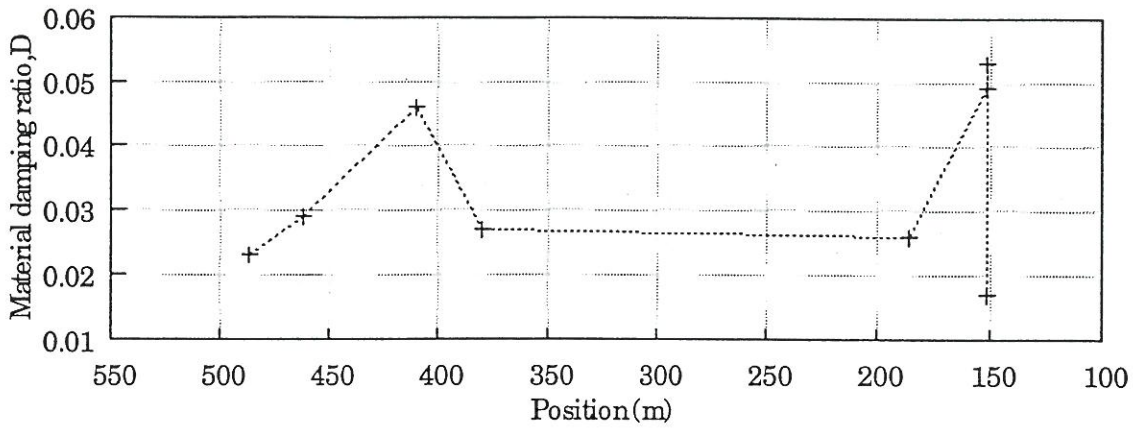

Fig. 4.12 Values for the material damping ratio, D, determined at the in situ stress for samples from 2 and 4.5 m's depth.

Evaluation of results from laboratory tests

The results from the laboratory tests does not show any significant difference in the results along the seismic line from the south to the north. The observed differences are more related to the difference in the soil structure (sandy or clayey sediments) than to the position along the seismic line. Values for the S-wave velocity, v_s, determined from the laboratory tests correspond very well to the values for the S-wave velocity as found by the seismic investigation in the field. The P-wave velocity, v_p, is very difficult to determine in the laboratory, since the variation of v_p with Poisson's ratio, μ, is so great, that μ has to be determined with an accuracy of 10^{-4}, which has not been possible in the actual tests.

If a soil is not saturated with water, but the voids contain small amounts of gas, it would not affect the value of the S-wave velocity and the shear modulus, but the values for Young's modulus and the damping ratio would be largely affected.

The actual laboratory tests have not shown any significant difference in the dynamic soil parameters along the seismic line. If, however, the voids have contained gas, when the samples were extracted from the soil, the gas would disappear during the consolidation process since the all round pressure was established by vacuum. An investigation to confirm the theory of gassification in the sediments was therefore carried out (see section 5).

5 Vane tests, Cone Penetration Tests and Soil gas measurements

Vane tests

In connection with the borings A and B, vane tests have been carried out to determine the undrained shear strength, c_v, of the clay sediments. The results of these tests are shown in fig. 5.2 and fig. 5.3. Vane tests have also been carried out in 2.2 m's depth below the surface in 10 positions along the seismic line. The results of these tests are shown in fig. 5.1. As seen from the figure relative high values for c_v are found in station 358 and station 380.

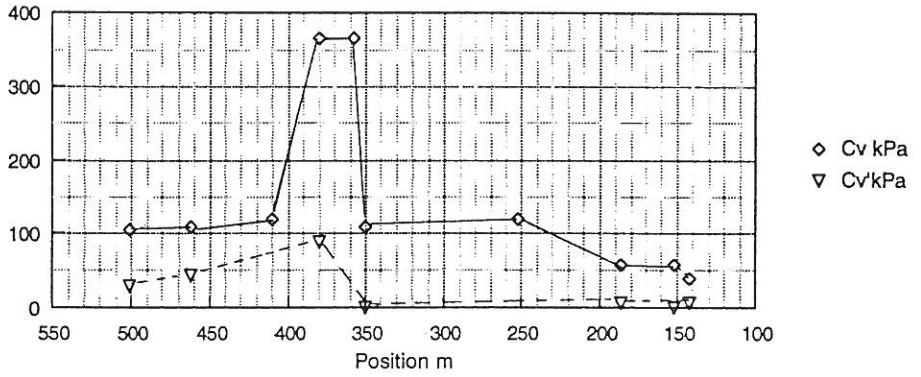

Fig. 5.1 Results of vane tests from 2.2 m's depth along the seismic line.

Cone Penetration Tests

The CPT-equipment used in the actual investigation was the van den Berg system developed in Holland. The cone is a piezo-cone. During the test the following values are measured:

1) q_c	= the cone resistance	- the penetration resistance on the tip
2) f_s	= the sleeve friction	- the side friction resistance on a friction sleeve
3) u_T	= the pore water pressure	- the pore water pressure present just above the cone shoulder is measured during the penetration

In sand deposits the cone resistance is high and the sleeve resistance low, in clay deposits the sleeve resistance is high compared to the cone resistance. The measured results from CPT's carried out close to the borings A and B are shown in fig. 5.2 and fig. 5.3.

From the measured results the friction ratio $f_r = f_s/q_c$ is calculated. In sand deposits the cone resistance is high, the friction ratio and the pore pressure low. In clay deposits the cone resistance is relatively low, the friction ratio and the pore pressure high. In clay deposits the undrained shear strength can be estimated from the cone resistance, the value is of the order of 1/10 of the cone resistance (Luke, 1994, Thorsen & Mortensen, 1995). Estimation of the minimum values of the field vane shear strength should be based on the determined values of the friction ratio (Luke, 1994).

The results of the borings and the CPT's in station 152 and station 486, respectively, are correlated, see fig. 5.2 and fig. 5.3. On the basis of these results an estimation of the soil classification is made from the results of the CPT's carried out along the seismic line. The results are shown in fig. 5.4.

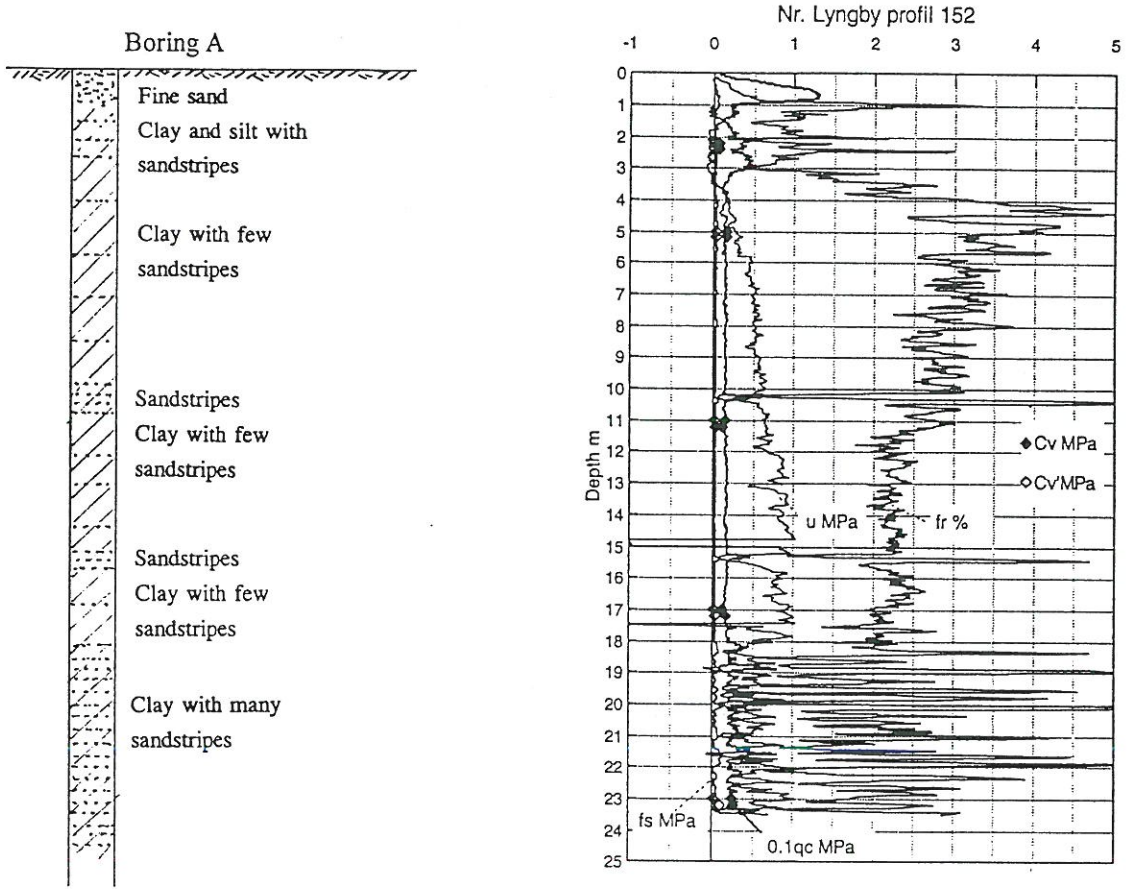

Fig. 5.2 The upper 25 m of boring A and the results of CPT in station 152.

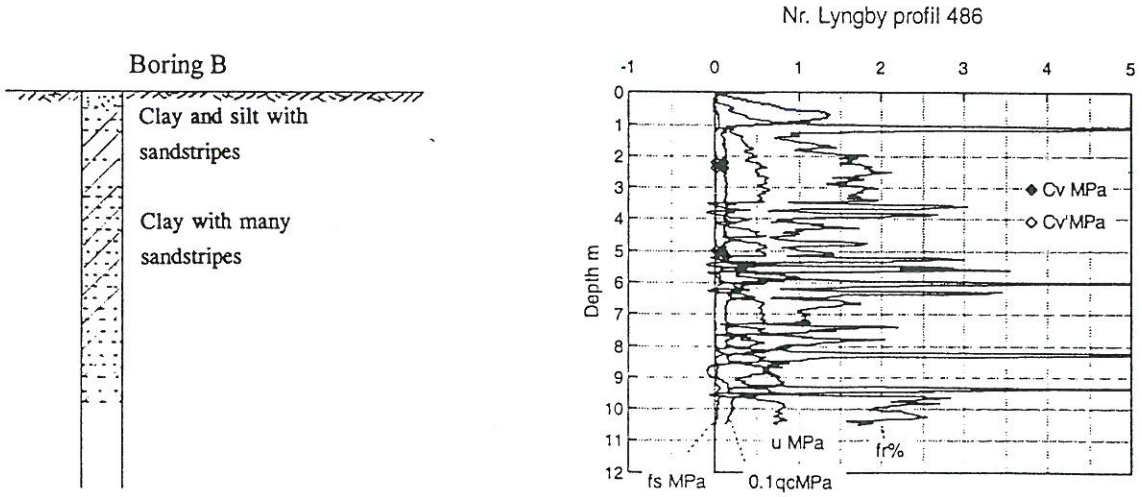

Fig. 5.3 The upper 12 m of boring B and the results of the CPT in station 486.

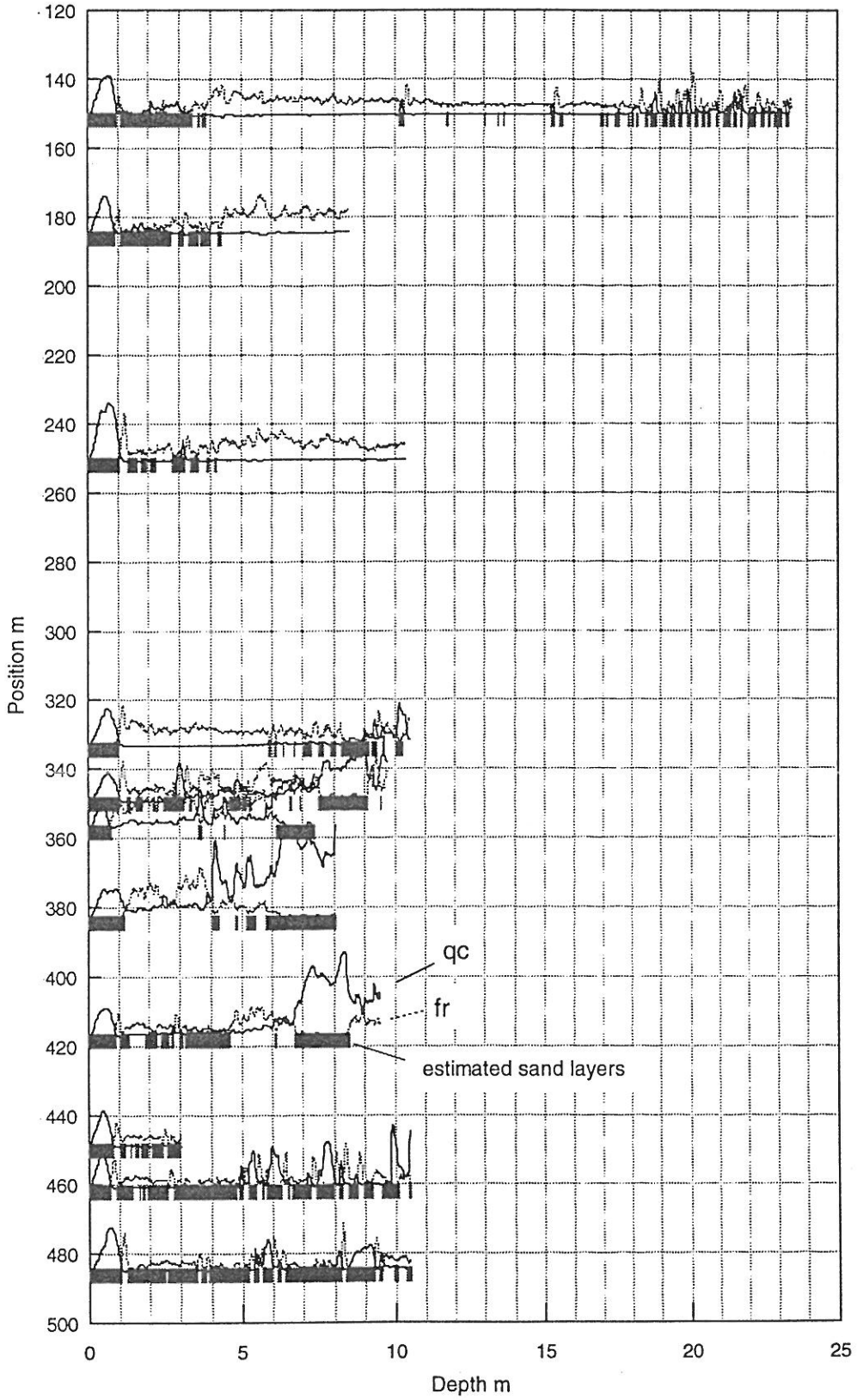

Fig. 5.4 Results from CPT, q_c and f_r, and estimatied sand layers from the CPT-results.

Soil gas measurements

With the Cone Penetration Test (CPT) equipment continuous soil gas measurements have been carried out at 16 positions along the seismic line. The soundings were taken to a depth of 8 - 15 meters below the surface. The purpose of the investigation was to analyse for gassification in the sediments.

The actual investigation has been carried out by the Danish consulting company Kampsax Geodan. With CPT tools developed for environmental investigations is it possible to carry out continuous soil gas analyses with the CPT equipment. The concept is to pump soil gas up through analysing instruments while penetrating the sediments and hereby determine the presence and concentrations of different types of gasses in the porewater.

In the actual investigation continuous analyses have been performed for methane, carbon dioxide and oxygen during penetration. In some of the soundings a considerable amount of methane has been found. The position of the soil gas soundings are shown in fig. 5.5, and the soundings in which methane is registered are marked.

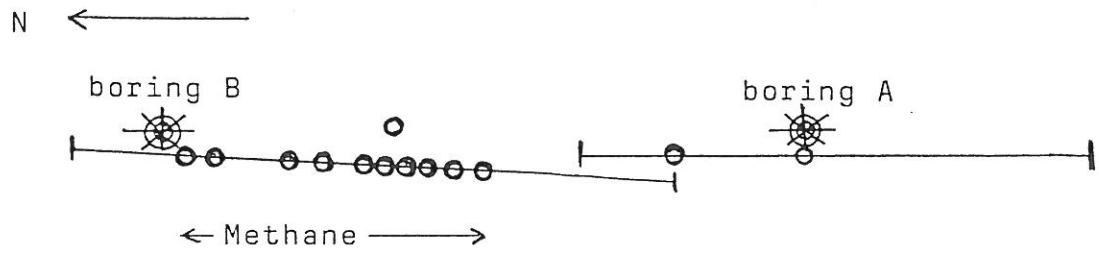

Fig. 5.5 Position of the soil gas soundings and the area in which methane is registered.

In some of the soundings a considerable amount of methane is registered and the methane seems to be concentrated in certain levels. Fig. 5.6 shows the results of a soil gas sounding and a CPT carried out in position 375 and 384 respectively. These results indicate, that the methane is concentrated in the sand layers.

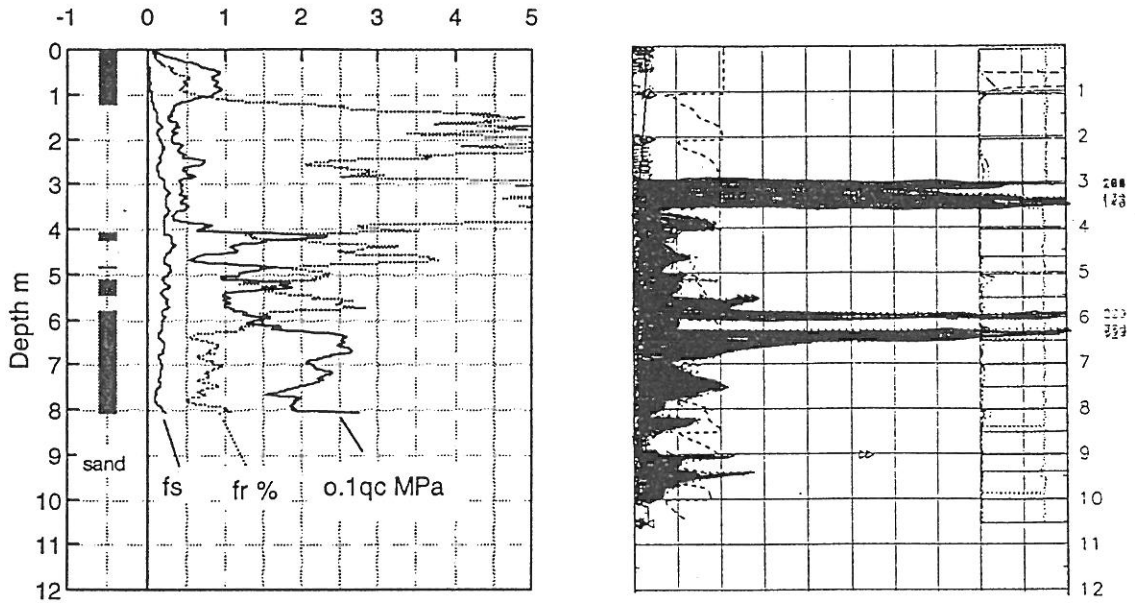

Fig. 5.6 Results from CPT in station 384 and soil gas measurements in station 375

Correlation between the CPT's and the soil gas soundings

The results of the measured value of q_c and the calculated value of f_r for the CPT's from station 300 to station 500 are shown in fig. 5.7 together with the estimated levels of sand layers and the levels in which methane has been registered by the soil gas soundings.

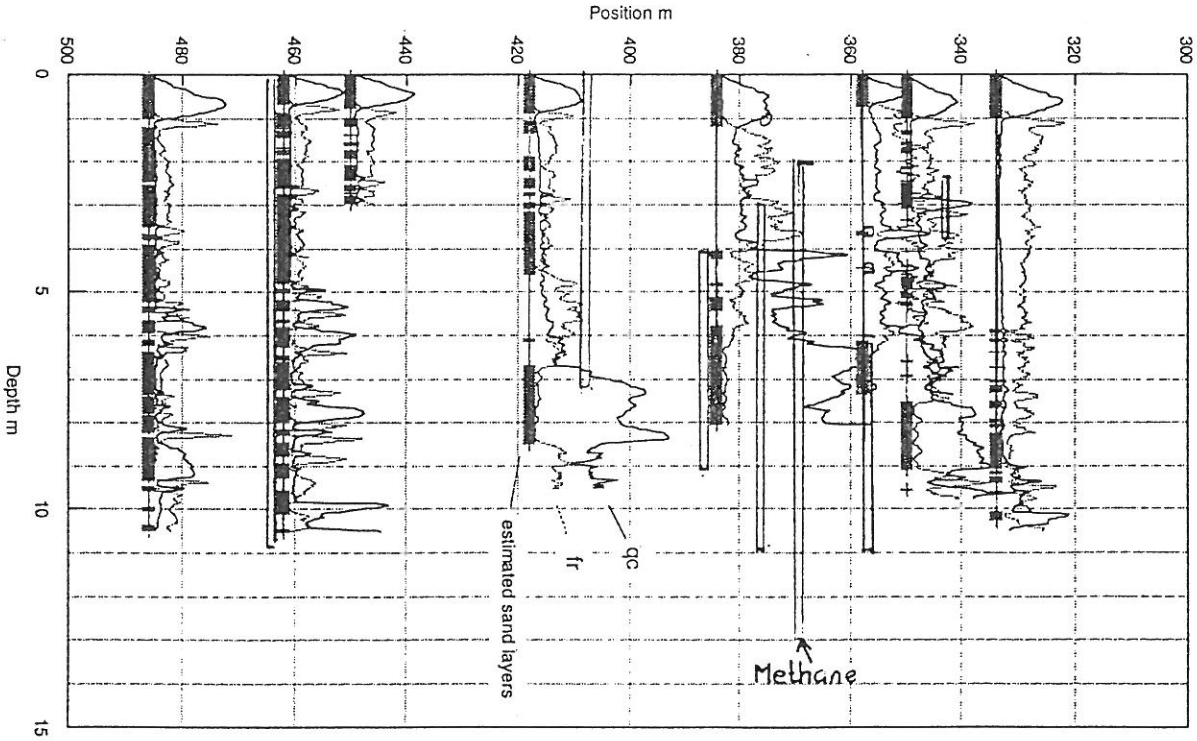

Fig. 5.7 Results of the CPT's, estimated sand layers and registered methane. Station 300 to station 500

6 In-situ seismic measurements

In order to verify the results of the laboratory tests and in order to examine if they apply to field conditions, a number of in-situ seismic measurements have been conducted. These include VSP measurements, S-wave refraction measurements, and experiments for monitoring the direct S-wave as function of depth by a technique developed under the present project.

Near surface P-wave velocities

A good estimate of the variations in the near surface P-wave velocities can be obtained from the first break information in the shallow reflection seismic data. By determining these velocities it has been observed, that the P-wave velocities vary between 1600 m/s and 1700 m/s along line 1 and between 1550 m/s and 1600 m/s along most of line 2. However, in an interval between Sta. 360 and 430 along line 2 significantly lower P-wave velocities have been estimated, which correlate with the interval where methane gas has been detected. The velocities vary in this place between 1200 and 1350 m/s. Since good correlation between the gas content and P-wave velocities exists, the low velocity zone is undoubtedly caused by gas.

VSP experiments

In order to determine the P-wave velocities as function of depth and in an attempt to estimate the P-wave absorption, VSP experiments have been carried out in well A and well B. The experiments were conducted shortly after the casings had been placed, which might have caused the fill behind the casing not being fully consolidated. This has in some places caused poor acoustic contact from the formation to the receivers.

The source signals for the VSP measurements were generated by a boomer placed 6 m from the well in a water filled basin with dimensions of 3 m x 3 m x 1 m. By using a boomer, highly repeatable source signals have been obtained. However, due to technical problems the boomer was only applied in well B. Instead cap detonators were used in well A which were activated in a similar water filled basin. However, this did not produce more uniform source signals compared to shooting directly in the sediments. As receivers a hydrophone cable with 11 hydrophones with a receiver spacing of 2.0 m was used.

In Fig. 6.1 the VSP data from well B are shown. The seismic section is composed from several shots. Although a high resolution source has been applied, low frequency signals are observed. This can be assigned to the poor acoustic properties at this place, which also characterize the reflection seismic data. No reflections have been observed on the present data. From the direct P-wave the average velocity has been estimated to 1650 m/s. In the interval from 15 to 22 m it is observed that low amplitude P-wave arrivals are present, which are probably caused by poor contact from the formation to the casing. Therefore, a reliable estimate of the attenuation could not be conducted in well B. In Fig. 6.2 the VSP data from Well A are shown. As source cap detonators were used, which were placed in a water filled

basin 9 m from the well. A bandpass filter of 200 - 1000 Hz has been applied. It is observed that clear reflections are present at all depths, which can be correlated with the reflection seismic data. From the first break information the following interval velocities have been estimated:

Depth	One-way traveltime	Two-way traveltime	Interval Velocity
5.0 m			1610 m/s
19.5 m	12.0 ms	24.0 ms	1595 m/s
27.4 m	16.8 ms	33.6 ms	1693 m/s
39.1 m	23.6 ms	47.2 ms	1702 m/s
48.4 m	28.9 ms	57.8 ms	1705 m/s
61.7 m	36.7 ms	73.4 ms	1657 m/s
70.5 m			

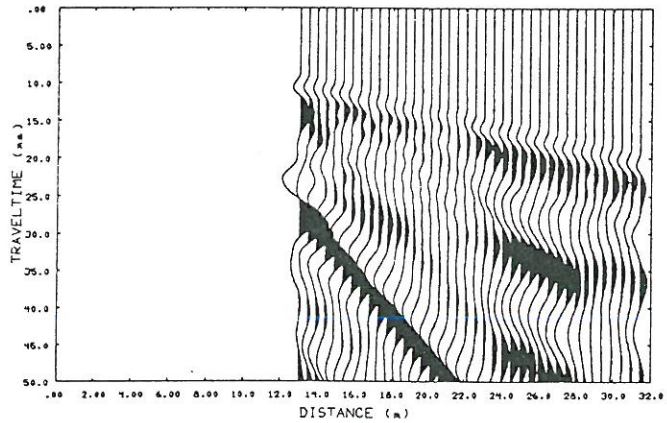

Fig. 6.1 VSP data acquired in Well B. A boomer placed in a water filled basin was used for generating the source pulse.

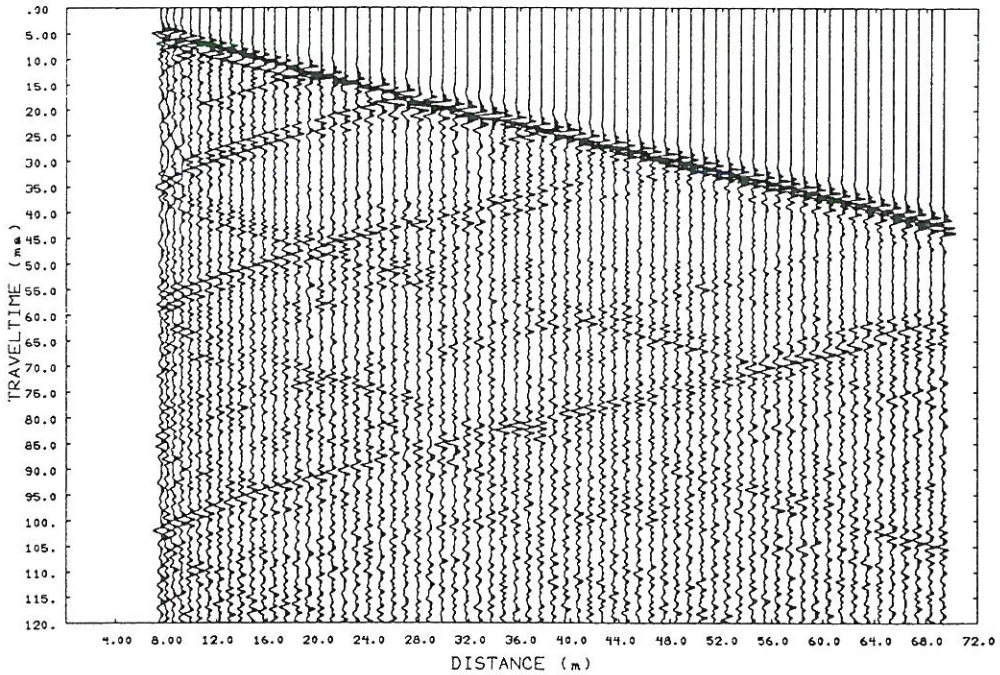

Fig. 6.2. VSP data acquired i Well A. The seismic traces are mapped as function of the source - receiver distance. Source: Cap detonators in a water filled basin.

P-wave attenuation estimated from VSP data

Only in the deepest parts of well A reliable P-wave attenuations could be determined. At other depths the variations in the amplitudes indicate a variable contact from the formation to the receivers, which is presumably caused by the fill not being sufficiently consolidated around the well. However, between 48 m and 68 m reliable data seem to be present. These data, which originate from the same shot, are shown in Fig. 6.3. The average attenuation in the present interval has been estimated to 0.5 dB per wave-length (Q=55), by use of the spectral ratio method. Q is the quality factor defined as $Q = 2\pi E / \Delta E$, with ΔE being the energy loss per cycle and E the energy used for elastic compression. In order to verify this attenuation downward continuation of the signal recorded at 48 m depth has been conducted. These signals are also plotted in Fig. 6.3. A constant velocity of 1657 m/s has been used for the downward continuation. Reflections have been ignored, which according to Fig. 6.2 is reasonable since no high amplitude reflections are observed in the present interval. Since scattering and transmission loss have not been taken into consideration, the actual attenuation might be lower (i.e. higher Q value).

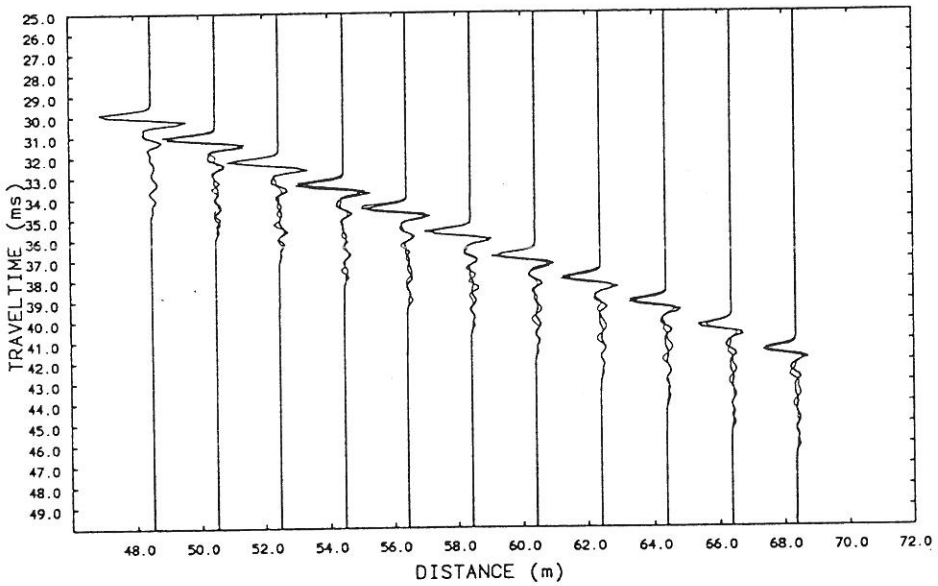

Fig. 6.3 Thin line: Tapered P-wave signals from the deepest parts of well A. Bold line: Downward continuation of signal recorded at 48 m with an absorption of 0.5 dB per wave-length (Q = 55). Both data sets have been compensated for spherical divergence.

S-wave refraction measurements

S-wave refraction measurements have been carried near well A and Well B. As source a hammer hitting a buried iron girder was used. The observations were made by three-component geophones in the offset interval from 5 m to 90 m and with a receiver spacing of 5.0 m. The SH-wave observations near well A and well B are shown in Fig. 6.4 and Fig. 6.5, respectively. Both the source signals and the horizontal receiver components are for these data orientated perpendicular to the refraction seismic profile.

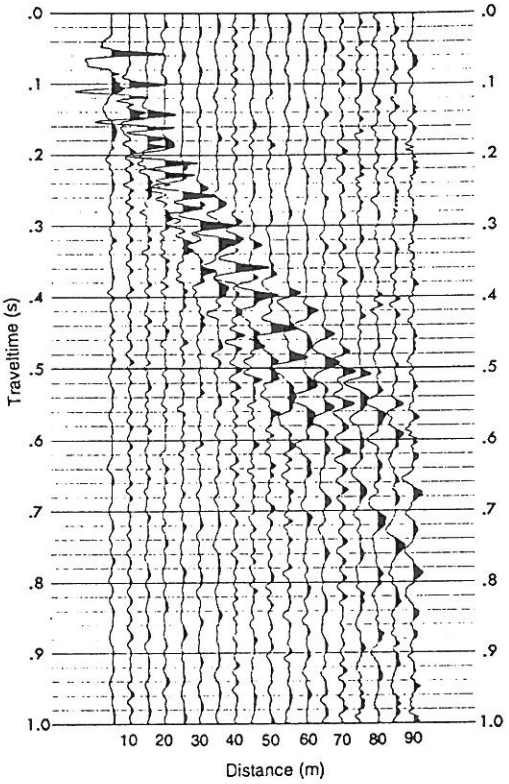

Fig. 6.4. Refracted S-waves acquired near well A.

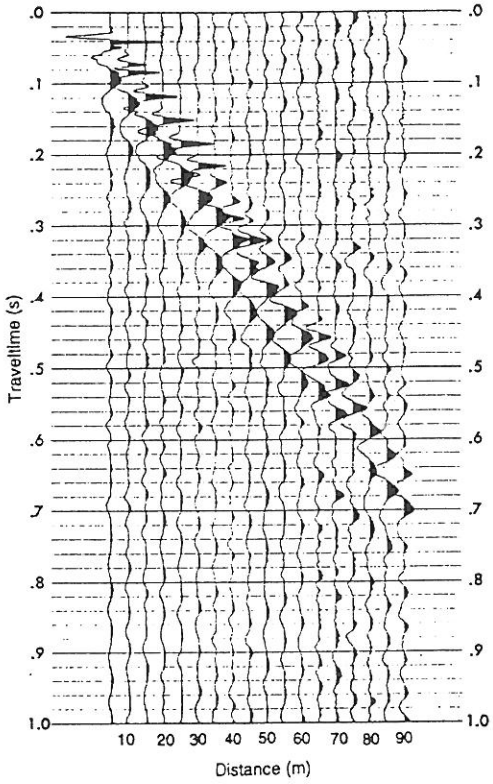

Fig. 6.5. Refracted S-waves acquired near well B.

The refraction seismic data from well A have been interpreted in a three layer model with velocities of 122 m/s, 169 m/s, and 240 m/s. The depth to the first refractor has been calculated to 5.0 m, and the depth to the second refractor has been estimated at 15.5 m, but the latter is uncertain due to only few observations at large offsets. The data from well B are interpreted in a two layer model with velocities of 146 m/s and 390 m/s and a refractor depth of 10.2 m.

Larger S-wave velocities along line 2 than along line 1 seem to be a consistent feature, which is also observed on shot gathers from the reflection survey, and by monitoring the direct S-wave as function of depth. The latter results will be described in the following section. The velocities being estimated compare reasonably well with the S-wave velocities estimated in the laboratory test (the bender elements test), which are described in section 4. Discrepancies between laboratory tests and field measurements are mainly expected to be caused by the different strain level being applied. The strain level for the laboratory tests are at least a magnitude higher than for the reflection seismic experiments.

In-situ measurements for estimating the S-wave attenuation

The present experiments have been conducted for estimating the attenuation of the near surface sediments. Surface observations of direct waves are not considered reliable for such experiments due to interferences from shallow reflections and surface waves, and due to the disturbing effect from unconsolidated sand close to the surface.

Previously, promising results of estimating the S-wave attenuation as function of depth have been reported by Stewart and Campanella (1993) using downhole seismic cone penetrations. In our experiments we have also concentrated on estimating the direct S-waves by depth, because good results have previously been obtained, and because it is possible to produce a highly repeatable source wavelet, which is necessary for such experiments. Moreover, S-waves have shorter wave lengths than P-waves, which reduces the depth interval needed for estimating the attenuation.

Instead of using seismic cone penetration equipment it was decided to build a seismic accelerometer into a hollow auger bit stem. A horizontal orientated piezoelectric accelerometer (Brüel & Kjær Cubic Deltatron Accelerometer, type 4502) was used due to a very linear frequency response in frequency interval of interest. The disadvantage of accelerometers compared to geophones is that the sensitivity is lower by a factor of approximately 40. However, as the following results will demonstrate, signals could easily be detected to a distance of about 10 m.

For the initial tests (not presented here) a hammer source was used. However, man-powered hammer signals are relatively weak and not completely repeatable. Therefore, a large pendulum was constructed with a wire length of 4.0 and with a weight of 40 kg, which hits a 100 kg buried iron girder. By using this procedure a highly repeatable source wavelets could be generated. For field arrangement see also Fig. 6.6.

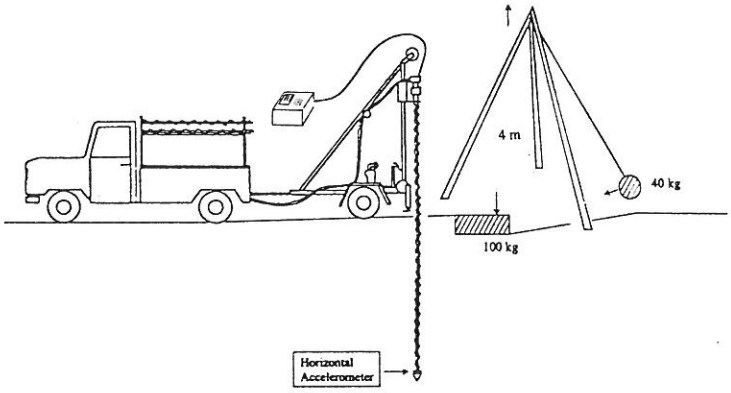

Fig. 6.6. Field arrangement for estimating the direct S-wave as function of depth.

In order to transmit the seismic signals to the surface a small amplifier was placed at the end of the drill stem near the accelerometer. Three soundings have been accomplished at Sta. 152, Sta. 495, and Sta. 374. The drill holes were placed approximately 1.0 m from the iron girder and measurements were made at depth intervals of 0.5 m. The data have all been compensated for spherical divergence. Otherwise, no processing has been applied except for a constant scaling on all traces. The soundings made near Well A (at Sta. 152), near Well B (at Sta. 495), and at Sta. 374 are shown in Fig. 6.7, 6.8, and 6.9, respectively. The traces are mapped as function of the distance from the source to the detector, and underneath the amplitude spectra of the tapered S-wave signals are shown. It is observed that S-wave signals

are well defined at all depths, except at shallow depth where the S-waves are not completely separated from other wave types. The direct P-waves are also observed but are not very consistent due to the fact that the source is not designed to generate this kind of wave.

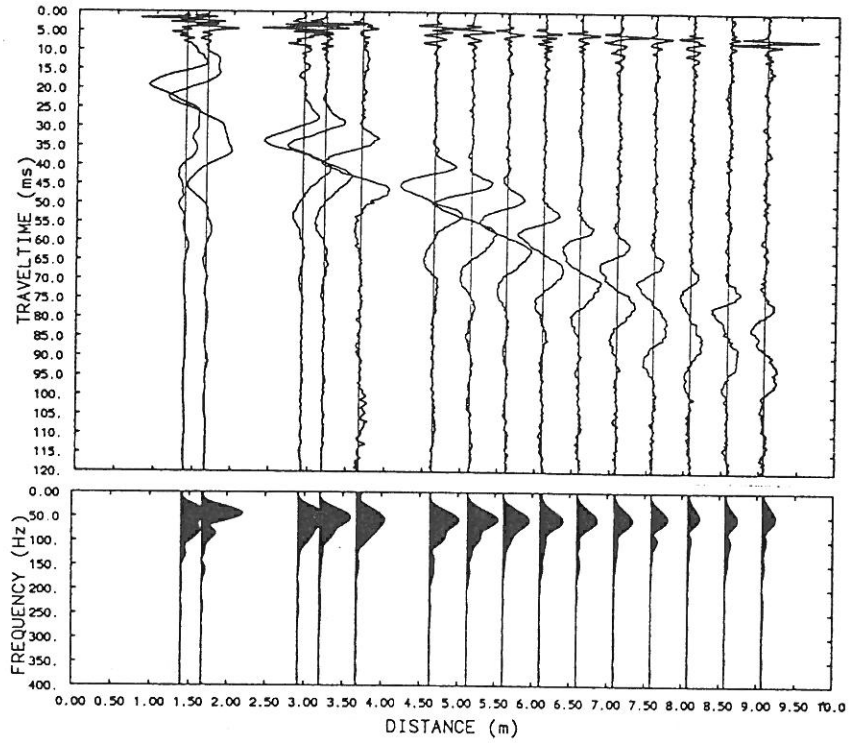

Fig. 6.7. Vertical seismic sounding near Well A (Sta. 152). The amplitude spectrum of the tapered S-waves signals are shown underneath.

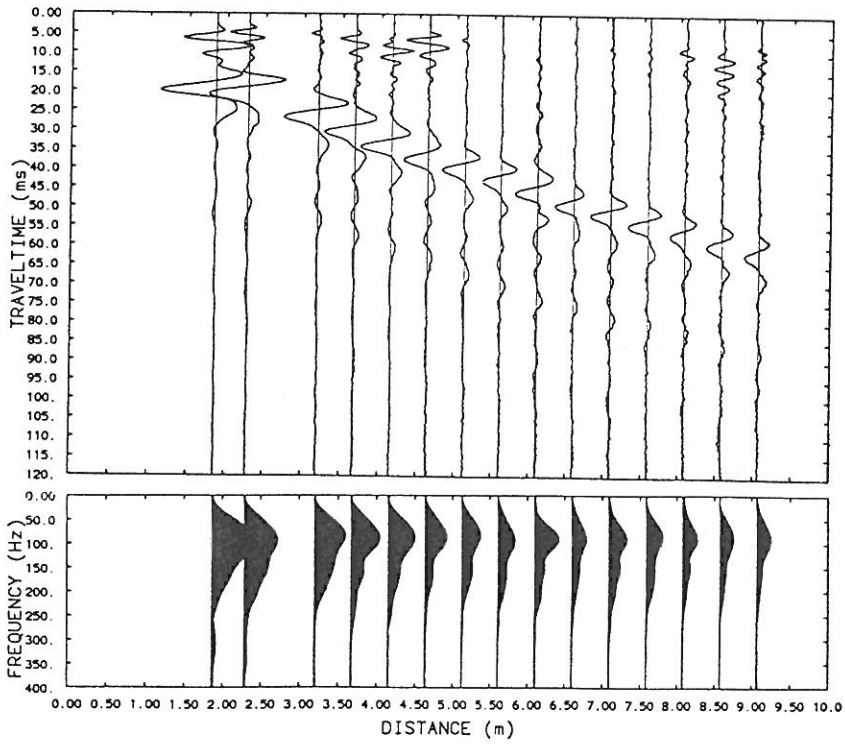

Fig. 6.8. Vertical seismic sounding near Well B (Sta. 495).

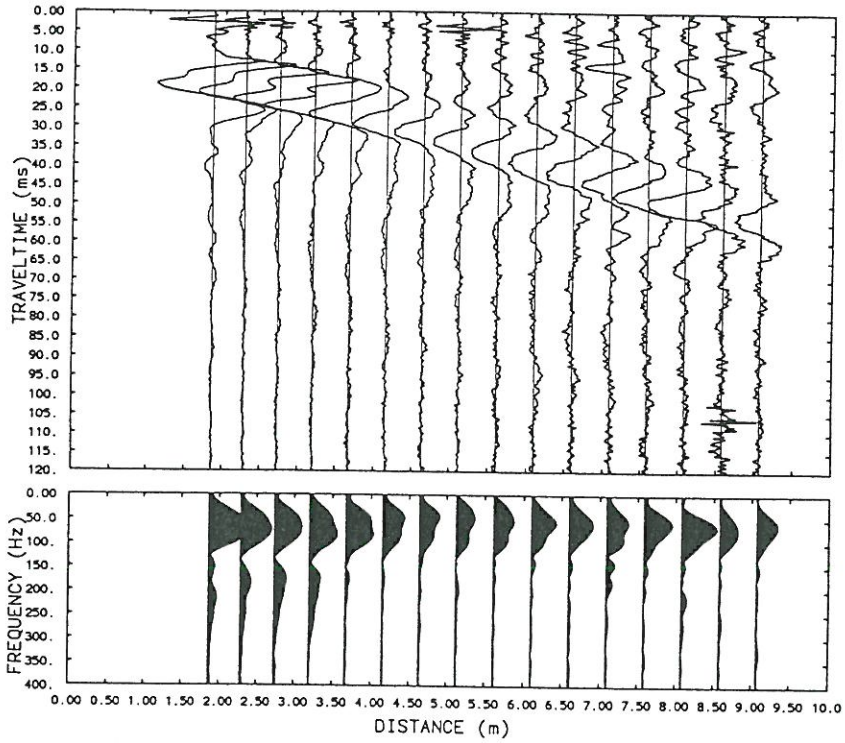

Fig. 6.9. S-wave sounding at Sta. 374.

At Sta. 152 generally lower frequencies are observed compared to the signals recorded at Sta. 495. The reason for this is probably the coupling from the iron girder to underlaying material. At Sta. 152 the sand was fully saturated which may have caused the iron girder not being fixated as well as on the other location, and consequently lower frequencies have been generated.

The S-wave velocity for the sounding at Sta. 152 is estimated to 120 m/s. At Sta. 495 the velocity from the surface to 7.0 m has been determined to 155 m/s, and below this level it has been estimated to 190 m/s. These results compare to the velocities estimated from S-wave refraction experiments.

At Sta. 374 a significantly higher S-wave velocity of 208 m/s has been estimated. The high S-wave velocity at Sta. 374 is also suggested by high shear strengths estimated by vane tests at 2.0 m depth. High S-wave velocity and high shear strength are presumably caused by calcium carbonate precipitated at shallow depth. The extent of the interval with high shear strength, seems to correlate with the interval where low P-wave velocities of near surface sediments have been estimated and with the interval with high gas content being detected. Since these intervals coincide, it is reasonable to assume that the anomalous acoustic parameters all are influenced by the high concentrations of methane. However, the interrelation between these phenomena are not yet fully understood.

In order to estimate the S-wave attenuation from the observations described above it is assumed, that the sediments are fairly homogeneous, which seem to apply to recordings at Sta. 152 and at Sta. 495. A taper is placed around the S-wave signals, the spectral amplitudes are found, and the attenuations are determined by use of the spectral ratio method. At Sta. 152 the attenuation is estimated to 2.6 dB per wave-length (Q = 10.5) and at Sta. 495 to 2.4 dB per wave-length (Q=11.5). Thus, almost no difference in the S-wave attenuations is present for the two places. However, it should be noted that these values are mainly based on signals below 120 Hz. At these low frequencies no significant difference in the P-wave signals attenuation has been detected either, cf. section 2. In order to verify the attenuations being estimated, downward continuation of signals recorded at shallow depth has been made. The absorption-dispersion relation by Nielsen (1978) has been used. Transmission loss due to reflections has not been taken into consideration. The results are shown in Fig. 6.10 and Fig. 6.11 together with the tapered S-wave observations. It is seen that the amplitudes and the wave forms of the downward continued signals are in good agreement with the observations.

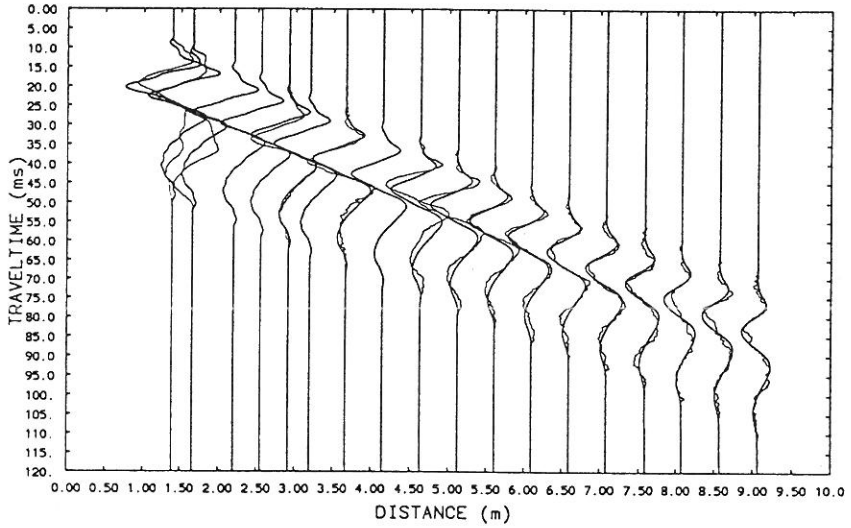

Fig. 6.10 Downward continuation of shallow S-wave signals recorded near Well A. The tapered S-wave observations are imposed.

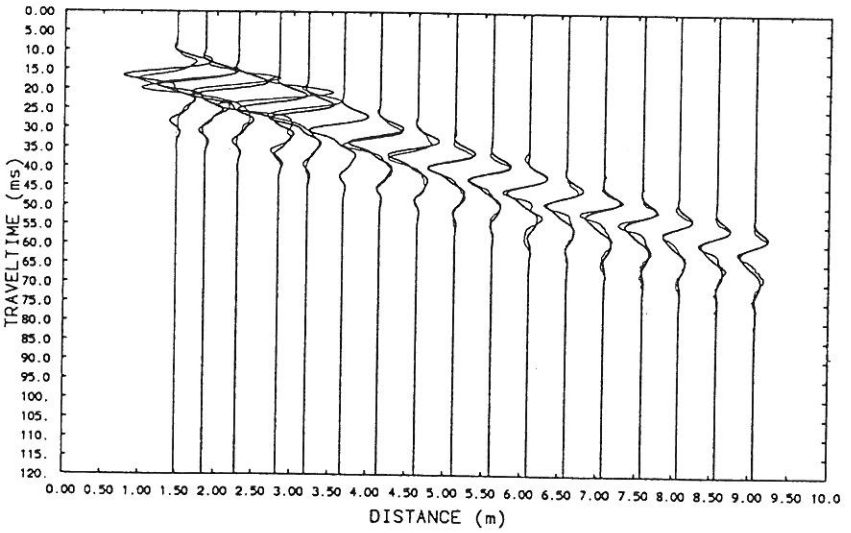

Fig. 6.11 Downward continuation of shallow S-wave signals recorded near Well B. The tapered S-wave observations are imposed.

The average S-wave attenuation at Sta. 374 compares to the attenuation being estimated near well A and B. However, the assumption of a homogenous formation is poor at this position. This is evident at distances between 3.2 and 3.7 m (i.e. depth of 3.0 and 3.5 m), where almost all high frequency signals above 130 Hz are eliminated. Closer to the surface no excessive attenuation of high frequency signals is observed. The depth interval (3.0-3.5 m) correlate perfectly with the interval where high concentration of methane gas has been detected at Sta. 375, cf. section 5. By estimating the attenuation in the present narrow interval, an extremely high attenuation of 27 dB per wave-length ($Q < 1.0$) is obtained.

7 2-D Wavefield modelling in absorbing layered media

The seismic experiments presented above have demonstrated, that absorption has a significant influence on the character and in particular the spectral content of reflection seismic data. In order to simulate seismic data in absorbing media a modelling technique has been developed, which makes it possible to include absorption and dispersion. The modelling routine, which is a spectral method, is confined to isotropic layered media. The simulation program is mainly aimed at P- and SV-wave modelling, but acoustic modelling can also be accomplished. The system is developed in cooperation with Professor Peder Hedebol Nielsen, Department of Earth Sciences, Aarhus University.

Spectral wavefield modelling has previously been described by e.g. Ganley (1981) and Kennett (1979). The main advantages of using this kind of modelling procedures are, that it is relatively easy to incorporate absorption and dispersion into the wavefield estimation, and the implementation is fairly uncomplicated when layered media are considered.

At $z = 0$, the x or z component of the displacement field (u_x, u_z), as function of time t and distance x, can be expressed by

$$u(x,t) = \int_{-\infty}^{\infty} \int_{-\infty}^{\infty} U(k_x, \nu) \exp(2\pi i(k_x x - \nu t)) d\nu dk_x$$

where $U(k_x, \nu)$ is the Fourier transform of $u(x,t)$. ν is the frequency and k_x the x-component of the wavevector $\bar{k} = (k_x, k_z)$. The modelling is based on estimating $U(k_x, \nu)$, which is transformed into the time-space domain. In practice a discrete Fourier transformation is applied through a Fast Fourier Transformation (FFT). This implies that a periodic solution in both space and time is found with period length (in terms of samples) of N_x and N_t. This will appear as if a pattern of source points are present at "distances" N_x and N_t apart. Later it will be discussed how this undesirable periodicity can be suppressed.

Each Fourier component $U(k_x, \nu)$ can be associated with a plane harmonic wave with frequency ν and wavenumber k_x, which at a given depth z can be expressed by

$$U(k_x, \nu)\exp(2\pi i(k_x x + k_z z - \nu t))$$

By inserting in the wave equation it is evident that

$$k_z = \pm\left(\frac{\nu^2}{V^2} - k_x^2\right)^{1/2}$$

V is either the P-wave velocity V_P or the S-wave velocity V_S depending on which type of wave is considered. In case of evanescent waves or waves in absorbing media k_z becomes complex. The imaginary part of k_z will then describe the attenuation in the $z$direction. When k_z is complex the sign is chosen, so that the absorption is applied in the direction of the wave propagation.

The absorption is introduced by defining complex modulus (relating stress and strain), which also implies complex velocities. Consider for simplicity the acoustic case and the modulus of compression: $\alpha(\nu) = \alpha_R(\nu) + i\alpha_I(\nu)$. According to Nielsen (1978) $\alpha(\nu)$, which ensures that causality is obtained, can be expressed by

$$\alpha_R(\nu) = K + \frac{2\mu}{\pi}\ln\left|\frac{\nu}{\nu_0}\right| \qquad \alpha_I(\nu) = \begin{cases} -\mu & \nu > 0 \\ \mu & \nu < 0 \end{cases}$$

where $K = V^2\rho$ is the modulus of compression at a given reference frequency ν_0 . μ is the absorption which ensures constant energy loss per cycle, and ρ is the density. The complex velocity C is determined as $\alpha(\nu) = C^2\rho$ which is inserted into the expression for k_z above. Thereby, the imaginary part of k_z will carry the absorption properties.

As an example of the absorption-dispersion relation above, the impulse response in a medium with a P-wave velocity of 1000 m/s and the absorption 1 dB/wavelength is given for various distances, cf. Fig. 7.1.

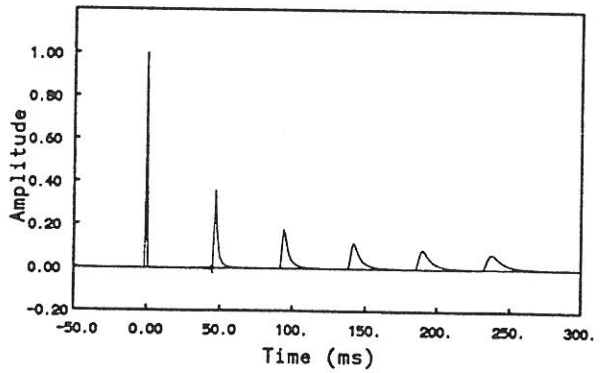

Fig. 7.1. Impulse response at the distances 50 m, 100 m, 150 m, 200 m, 250 m.

Wavefield propagation

Wavefield propagation in layered media is uncomplicated for constant k_x and ν (i.e. plane waves) and can be described by two processes, namely upward/downward continuation of the wavefield and wavefield estimation across layer boundaries.

In the frequency-wavenumber domain the upward/downward continuation is carried out by complex multiplication of $U(k_x, \nu)$. A displacement Δz of $u(x,t)$ is in the frequency-wavenumber domain accomplished by multiplying $U(k_x, \nu)$ by $\exp(2\pi i k_z \Delta z)$.

Estimation of wavefields across layer boundaries is conducted as follows: Let $U(k_x, \nu)$ of the upgoing and downgoing P- and SV-waves at one side of a layer boundary be known. In order to determine the spectral wavefield components on the other side of the layer boundary, continuity of the displacement vector and continuity of normal and shear stress is required, which in the modelling program is achieved by solving a linear equation system. When passing layer boundaries it is utilized that k_x is constant over a layer boundary (according to Snell's law). Since ν is also unchanged k_z is readily obtained as described above. k_z is needed in the expression of normal and the shear stresses which are estimated by use of Hooke's law. In case of a layer baoundary with an elastic layer on one side and an acoustic layer (with $V_S = 0$) on the other side, only continuity of normal stress and u_z is required. Thus slippage can occur across such layer boundaries. Finally, in case of a free surface, stress free conditions at the surface must be achieved.

Source spectrum

Before the wavefield modelling is initiated the source spectrum $S(k_x, \nu)^{uP}$, $S(k_x, \nu)^{dP}$, $S(k_x, \nu)^{uS}$ and $S(k_x, \nu)^{dS}$ of the upward and downward travelling P- and SV-wave must be defined. Index u and d refer to the direction (up and down) of the wavefield and P and S to the wave type.

Unfortunately, it is relatively complicated to define spectra for most sources with given physical properties, even in relatively simple cases. However, the source used in the present context, a P-wave line source emitting the same pressure in all directions, is relatively uncomplicated. According to (Båth, 1968) point/line source with "unit intensity" (in terms of pressure or displacement) has the spectrum $S(k_x, \nu) = i / k_z$. However, it should be noted that horizontally travelling waves cannot be generated, because such waves are not treated in the present kind of modelling methods.

Modelling technique

In order to calculate synthetic seismograms four subsolutions are joined. Solutions No. 1 and 2 are estimated by making upward continuation of downgoing P- and SV-waves, which are initiated in lowermost layer, as shown in Fig. 7.2a and 7.2b. Solutions No. 3 and 4 are found in the same way but by making downward continuation of upgoing P- and SV-waves, which are initiated in the uppermost layer boundary above the source and receiver level, cf. Fig. 7.2c and 7.2d.

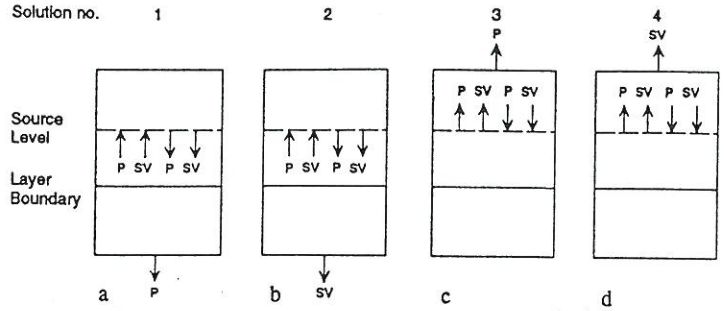

Fig. 7.2. The desired source spectrum is achieved as a linear combination of solution 1-4. The wavefields in solutions 1-2 are estimated by making upward continuation of a downgoing P- and SV-waves, initiated in the lowermost layer (a and b). The wavefields in solutions 3-4 are achieved in the same way but by starting in the uppermost layer instead (c and d).

Let the spectral amplitudes at the source level in solution i be denoted $A(k_x,\nu)_i^{uP}$, $A(k_x,\nu)_i^{dP}$, $A(k_x,\nu)_i^{uS}$ and $A(k_x,\nu)_i^{dS}$. In solutions 1 and 2 it is assumed that no waves are present above the source level, and similarly in solutions 3 and 4, it is assumed that the sources annihilate the wavefields below the source level. The source in solutions $i = 1$ and $i = 2$ which possess these properties, must have the spectral components:

$S(k_x,\nu)_i^{uP} = -A(k_x,\nu)_i^{uP}$,

$S(k_x,\nu)_i^{dP} = A(k_x,\nu)_i^{dP}$,

$S(k_x,\nu)_i^{uS} = -A(k_x,\nu)_i^{uS}$ and

$S(k_x,\nu)_i^{dS} = A(k_x,\nu)_i^{dS}$

Now a linear combination of source signals in solutions 1-4 is made so that after scaling and superposition the desired spectrum is obtained.

In order to determine the synthetic seismograms it is assumed that the wavefields at the receiver level in the different solutions have been recorded. The spectral component of the synthetic seismograms is achieved as a linear combination of these wavefields according to the scaling determined for source signals. When all spectral components are determined a 2-D FFT is applied so that the solution in the space-time domain is achieved.

In order to obtain numerical stability and to keep the spectral amplitudes within a reasonable dynamic range, the P- and SV-wave components are zeroed if the amplitude of both wave types is reduced by more than a given factor when penetrating a certain layer. In that case new downgoing P- and SV-waves (when considering solutions 1 or 2) are initiated after the layer in question has been passed. This procedure is aimed at evanescent waves which are not able of penetrating a layer with a reasonably large amplitude.

In case of evanescent P-waves, but non-evanescent SV-waves, resulting in only the P-waves being reduced by more than the specified threshold value, a linear combination of solution 1 and 2 is made, so that the upgoing P-waves are eliminated. Next, the SV-waves from 1 and 2 are joined, and after the layer has been passed a new downgoing P-wave is initiated. This procedure requires that upward/downward continuations of solution 1 and 2 (or 3 and 4) are accomplished simultaneously.

Suppression of wrap-around effects

When discrete Fourier analysis is used, an undesirable periodicity is present, which makes the source appear as if it is periodic in both time and space. Normally, this periodicity is suppressed by applying large attenuations and by choosing sufficiently long periods for the Fourier transformation. However, this will cause unnecessarily long computational times. In the present implementation we suppress these periodic effects by including an artificial exponential attenuation in space and time, which can fully be compensated for after the Fourier transformation has been accomplished. This technique will strongly reduce signals from the neighbouring periods. The suppression of wrap-around effects can be applied independently of the real attenuation.

The idea of the present method is that instead of determining the displacement field for the periodic function $u(x,t)$ we seek the solution $u(x,t)\exp(-\alpha t/T)\exp(-|\beta x/X|)$. α and β are constants and T and X are the period lengths. If this can be achieved the neighbouring sources at "distances" $j_t T$ and $|j_x X|$ in time and space from the soure in the main period are suppressed by $\exp(-\alpha j_t)$ and $\exp(-|\beta j_x|)$, respectively. j_t and j_x are period indices, with $j_t = 0$ and $j_x = 0$ in the main period.

Consider, for simplicity, only the suppression of periodicity in time. Thus we seek the solution $u(x,t)\exp(-\alpha t/T)$ to the wave equation. This can be achieved by modifying the differential operator in the wave equation in such a way that the exponential factor is neglected. That is, we want to find the operator ∂', so that

$$\frac{\partial'\{u(x,t)\exp(-\alpha t)\}}{\partial t} = \exp(-\alpha t)\frac{\partial u(x,t)}{\partial t}$$

The operator $\partial' = \alpha + \partial/\partial t$ satisfies this condition. Thus $u(x,t)\exp(-\alpha t/T)$ is a solution to "the modified wave equation" and $u(x,t)$ is at the same time a solution to "the real wave equation". In frequency domain ∂' is $F(\partial') = \alpha + 2\pi i\nu$, where F denotes the Fourier transformation. The modification of the spatial differential operator is introduced in the same way. By applying the modified differential operators on a plane wave introduces the expression

$$(2\pi i k_z)^2 + (\beta + 2\pi i k_x)^2 = \frac{(\alpha - 2\pi i\nu)^2}{C^2}$$

from which k_z is now determined. In this way "the modified wave equation" is applied. After the spectral components to the exponentially damped solution has been found and after 2-D Fourier transformation to the space-time domain has been made, compensation for the exponential damping is carried out.

The effect of the exponential damping is demonstrated in Fig. 7.3 for $\alpha = 2$, where the exponential damping is shown in four periods. It is observed that compensating for the exponential damping in the main period will only partly recover signals from the neighbouring periods. For $\alpha = 2$ the signals from the first order neighbouring period will be reduced by a factor $\exp(-2) \approx 0.135$ and signals from the second order neighbouring period by $\exp(-4) \approx 0.018$. Thus, the periodic effects have been considerably reduced, and if any periodic events remain, only signals next to the main period are significant.

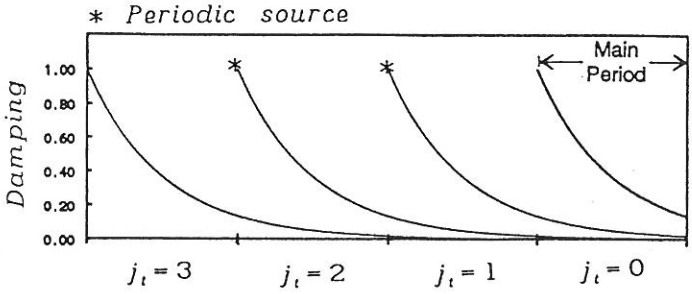

Fig. 7.3. Exponential damping of a periodic source. ($\alpha = 2$).

Example

The improvement by using the wrap-around suppression described above is demonstrated in the following example. The model being used consists of two layers with $V_P = 1000 m/s$, $V_S = 500 m/s$, and $\rho = 1000 kg/m^3$ in the top layer and $V_P = 2000 m/s$, $V_S = 1000 m/s$, and $\rho = 2000 kg/m^3$ in the bottom layer. No absorption is present in the model. The source level is at $Z = 5.0 m$ in uppermost layer, the receiver level at $Z = 0.0 m$, and the layer boundary is present at $Z = 15.0 m$. The source emits both upgoing and downgoing P-waves with a source spectrum as described above. A Ricker wavelet with a peak frequency of 150 Hz is imposed. A relatively shot period of 256 samples in both time and space has been chosen. In all examples the direct P-wave has been subtracted.

In Fig. 7.4a no wrap-around suppression is applied, which causes interferences from the neighbouring sources. In Fig. 7.4b wrap-around suppression with $\alpha = 3$ and $\beta = 2$ is applied, which eliminates most of the periodic effects. The remaining effects, which are mainly caused by sources next to the main period, have in Fig. 7.4c been removed by FK-filtering. It has been utilized that only signals with a positive inclination (beyond a certain offset) are present in the right part of the seismic section, and only signals with negative inclination are present in the left part of it. FK-filtering is simple to carry out in the present method because data are generated in the frequency wavenumber domain.

Comparison with a fourth order finite difference method

In order to test the results from the present spectral wavefield modelling, a comparison with a fourth order finite difference method by Levander (1988) has been conducted. The finite difference routine being used, has been implemented at Department of Earth Sciences, Universisty of Utah, by Yi Luo and Jerry Schuster.

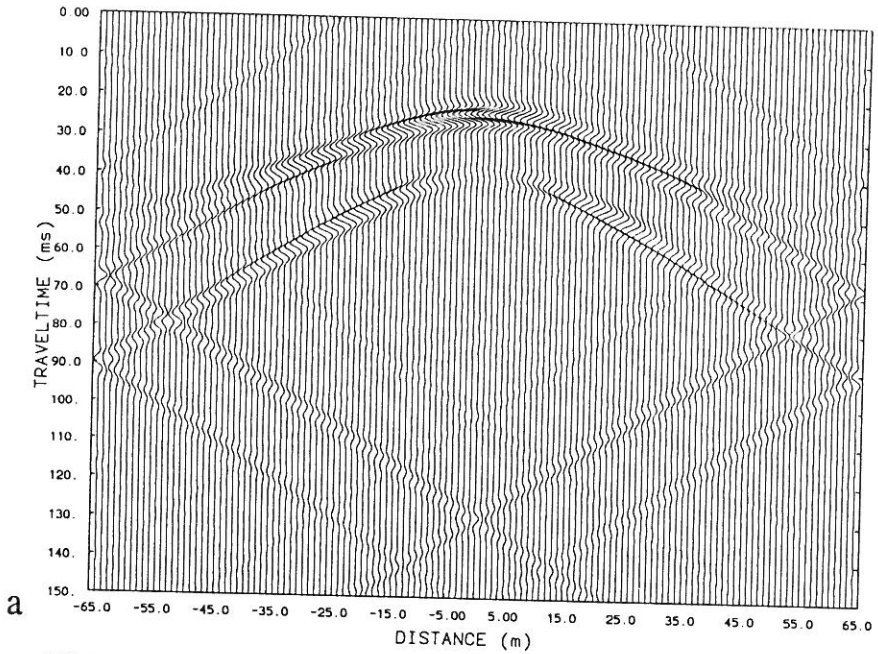

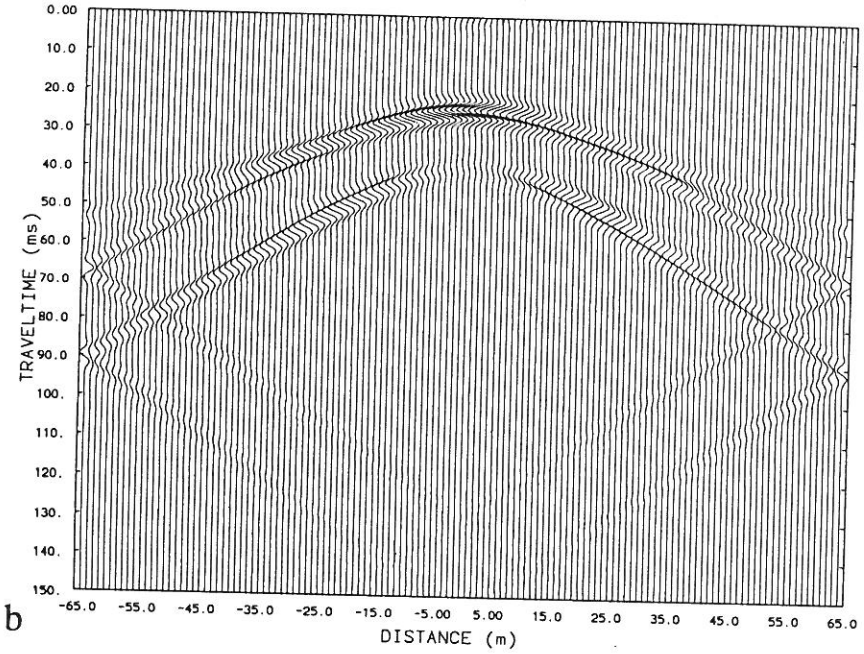

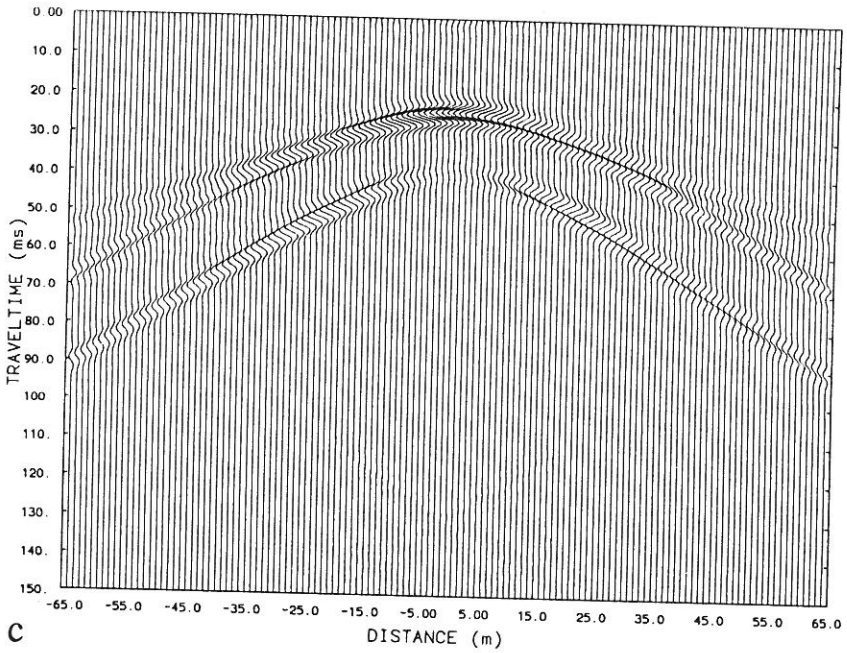

Fig. 7.4. Synthetic seismograms in a model with only one layer boundary. The first arriving event is the reflected/refracted P-wave. The following event is the P-wave converted to an SV-wave. The direct P-wave has been subtracted.

a) No wrap-around suppression.

b) Wrap-around suppression with $\alpha = 3$ and $\beta = 2$.

c) In addition to the wrap-around suppression in (b) FK-filtering has been performed.

The example from Fig. 7.4c has been used for the comparison. In both methods the direct P-waves have been subtracted. The comparison is shown in Fig. 7.5. The only significant discrepancies between the two wavefields are located for the P-wave reflection between 15 m and 25 m, which is probably caused by the FK-filtering, because a taper zone is present in this interval. At greater offsets a small displacement in time between the P-wave reflections are present. The reason for this displacement is unknown. However, in general good agreement between the two solutions are present, and it is our impression that much better results cannot be expected when two methods are compared, none of which is highly accurate.

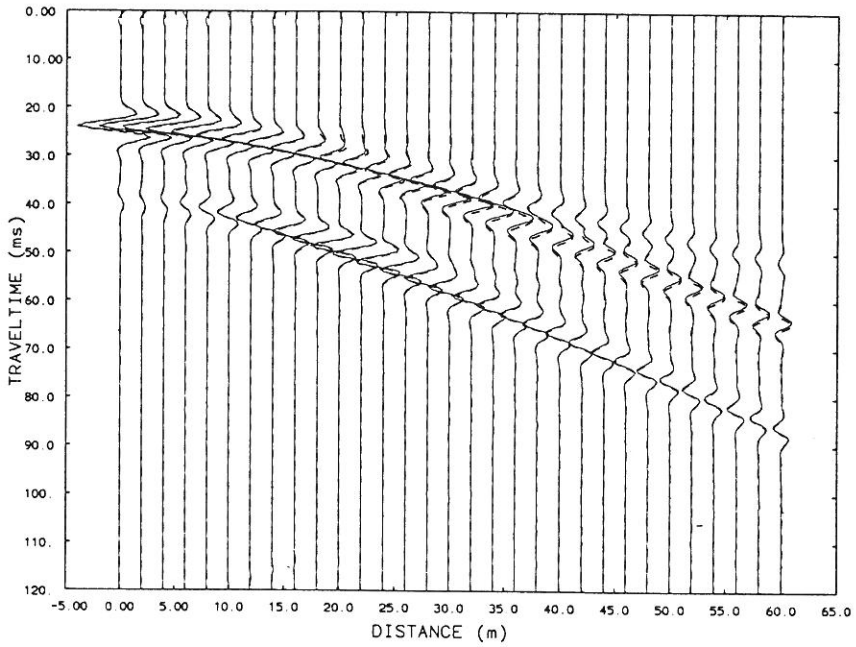

Fig. 7.5. Comparison between the present spectral wavefield modelling technique (bold line) and a fourth order finite difference method (dotted line). The model is the same as used in Fig. 7.4.

Modelling the transition zone at the Nr. Lyngby locality

As described in section 2 significant variations in the spectral content, are observed on shot gather acquired at the Nr. Lyngby locality, cf. Fig. 2.11. The changes take place in a narrow interval, which is only few meter wide. Amplitude spectra for shallow reflections at Sta. 353 and at Sta. 355 are shown in Fig. 2.12, which are positioned on either side of the transition zone, only 2.0 m apart. Significant attenuations from Sta. 353 to Sta. 355 have been observed for all charge sizes in use, i.e. cap detonator (C.D.), 8 g of compressed powder, 25 g, and 100 g of dynamite. As discussed in section 2 the attenuation has mainly affected signals above 120 Hz, for which the spectral amplitudes (at Sta. 353 and at Sta. 355) are also given in Fig. 7.6. For comparison the attenuation of a 300 Hz Ricker wavelet over a distance of 5.0 m in material with an absorption of 5 db per wave-length (Q = 5.5).

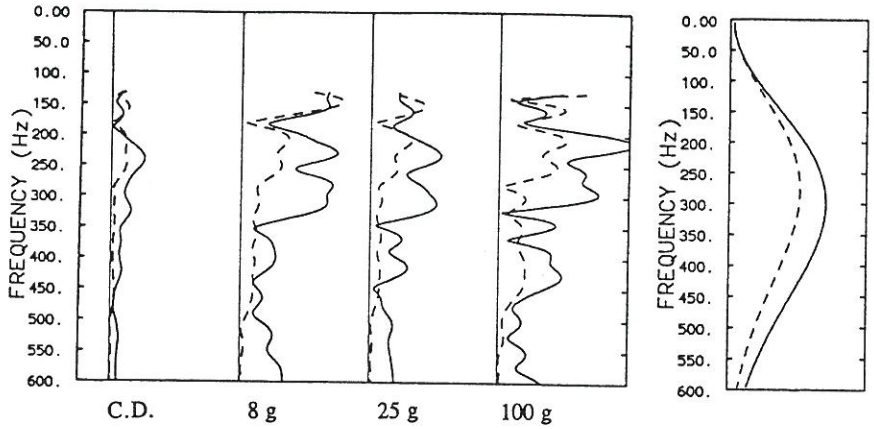

Fig. 7.6 Amplitude spectra for shallow reflections above 120 Hz for traces indicated in Fig. 2.11. The charge sizes are given underneath. For comparison it is shown how much a 300 Hz Ricker wavelet is attenuated over 5.0 m in material with Q = 5.5.

The reason for the high attenuation is most likely substantial amounts of the methane gas being detected in thin layers at depths from 3 m to 13 m between Sta. 357 to Sta. 410, cf. section 5. Near the present recordings at Sta. 357 gas has been found in the depth intervals: 6.75-8.00 m, 8.60-8.80 m, and 9.00-9.50 m. Thus, in total the sediments with high gas content cover about 2.0 m.

The source signal for the shot gathers shown in Fig. 2.11 are generated in late glacial sandy sediments, near the boundary of the erosional channel which was described in section 3. These layers are known to be thin at the shot point, so it is reasonable to assume that these sediments have only affected the source signals, which are characterized by unusually high freqeuncies.

From the cone penetration tests, which are described in section 5, it is reasonable to assume a fairly horizontal layering below the late glacial deposits. Reflections from these horizons are simulated by introducing thin layers with velocities between 1600 m/s and 1650 m/s in the depth interval from 8.0 m to 28.0 m. Layer thiknesses between 0.8 m and 2.4 m are assumed. The densities follow the variations in the velocities and are designated values between 2000 kg/m^3 and 2110 kg/m^3. Arbitrary variations in layer thiknesses, velocities and densities are used, because no detailed information about variations in acoustic parameters is recorded at this place.

The synthetic seismograms are estimated by the modelling technique described above. As source signal a 500 Hz P-wave Ricker wavelet is used. First, an absorption of 0.35 dB per wave-length (Q = 78) in all layers is assumed, which is inspired of the attenuation being estimated between 48 and 68 m in Well A. Although, the attenuation is estimated in another place, it is reasonable to assume a comparable attenuation here, because the sediments originate from the same formation. Next, the simulation is repeated with the uppermost 5.0 m below the receiver level being replaced by material with a high attenuation (5.0 db per wave-length or Q = 5.5). This layer is assumed to represent all thin layers with a high gas

content. These two data sets are merged and shown in Fig. 7.7. For comparison low-cut filtered reflections from the shot gather acquired by 8g of powder are given in Fig. 7.8. In both shot gathers a constant scaling on all traces has been applied.

The present simulation is not an attempt to make accurate simulations of details in the data, but has been carried out for evaluating the attenuation needed to eliminate the high frequency reflections north of Sta. 355. It is observed that the amplitudes and the character of the reflections in general compare reasonably well. In particular it is observed that beyond Sta. 355 only low frequency "ringing" is present, which cannot be related to any specific reflectors.

In the present simulation high attenuation in an interval about twice the total thickness of sediments with a high gas content has been applied. However, most of the gas is detected in relatively thin layers, less than 2.0 m thick. Thus, it must be concluded that the actual attenuation in those layers is bigger than 5.0 dB per wave-length ($Q < 5.5$). This agrees with the observations from the vertical monitoring of the direct S-wave, which were described in section 6, although the attenuation for P- and S-waves cannot be directly compared. The fact that the attenuation occurs in very thin layers may also explain, why signals with frequencies below 120 Hz, are almost unaffected by the attenuation.

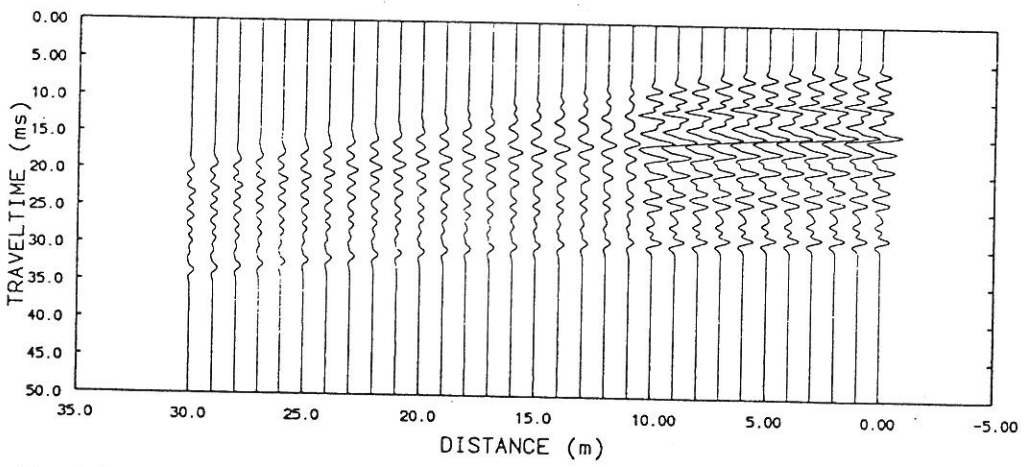

Fig. 7.7. Simulation of shallow P-wave reflections across the transition zone. The section is merged by results from two simulations. A contant attenuation of 0.35 db per wave-length is assigned to all layers. At offsets greater than 10.0 m a 5.0 m thick layer below the receiver level is introduced with an attenuation of 5.0 dB per wave-length.

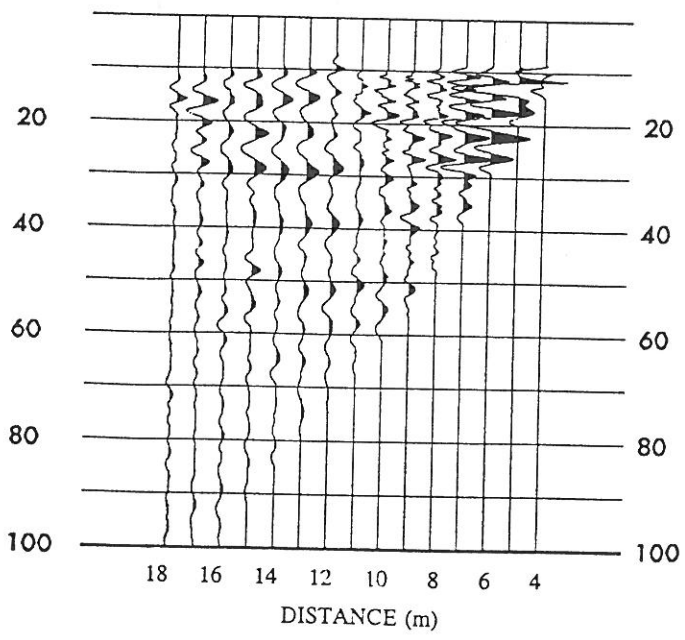

Fig. 7.8. Shallow reflections acquired by use 8 g of compressed powder. A low-cut filter and a constant scaling has been applied on all traces.

8 Conclusion

Severe variations in the quality of reflection seismic data have been demonstrated in two cases from Denmark in areas with unconsolidated surface sediments. These variations are mainly expressed in the spectral content, and particularly on shallow seismic data, where high frequency signals are employed. However, conventional seismic data are also affected, in spite of shots, which are preferably activated below the weathering layer, and in spite of larger charge sizes which result in lower frequencies.

On the location chosen for most of our research it has been demonstrated that transformation of seismic signals during the wave propagation, which primarily can be assigned to absorption, is of main importance and may alone be responsible for the variations in the data quality. However, variations in the source signals may be of significance, although it is difficult to evaluate when severe attenuation in the near surface sediments also takes place.

In order to determine the elastic properties of the sediments at our test locality, intact core sampling has been made in two wells and at 2 m depth along the seismic profiles. Resonance column tests for estimating Young's modulus and bender elements test for determining the shear modulus have been conducted. The results of the laboratory tests have not revealed any significant variations in the elastic properties, which can be correlated with the spectral content of the seismic data. Lithologically, the sediments are also quite similar, in spite of the fact that the sediments are of different ages. The S-wave velocities determined from the shear modulus compare reasonably well to the S-wave velocities estimated from refraction seismic data. The same kind of comparison was not possible for P-waves, because reliable velocities cannot be derived from Young's modulus for poisons ratio near 0.5. However, fairly good control of average P-wave velocities has been obtained from the VSP measurements.

The P-wave attenuation estimated from resonance column tests does not show any significant variations either. The attenuation varies between $Q=10$ and $Q=25$ when estimated from samples taken at depths between 2 m and 16 m. However, it should be noted that it is uncertain whether the attenuations apply to the conditions under which shallow seismic data are acquired, because significantly lower strain level is applied here. Still, the results seem reasonable when compared with the P-wave attenuation of $Q=55$, which has been estimated from the VSP measurements in the depth interval from 48 to 68 m. S-wave attenuations of $Q=10$ and $Q=12$ have been estimated by in-situ measurements as average values for the depth interval between 2.0 m and 8.0 m. These measurements are conducted by a technique developed under the present project, where the direct S-waves are monitored in a hollow auger bit drill stem as function of depth. On field observations it has been detected that significant variations in the attenuation of high and low frequency signals are present. Thus, signals above 120 Hz are attenuated much more than signals below 120 Hz over the offset range in question. This has been observed for different charge sizes, but is most pronounced for small charges, because they tend to focus on higher frequencies.

In the area where the most severe attenuation is present a high content of methane gas has been detected by continuous gas soundings conducted by cone penetration equipment. The intervals with high gas content are relatively thin, mainly between 0.5 m and 1.0 m thick, and has been detected at several levels between 3 m to 13 m depth. A perfect correlation between a high content of gas and a severe attenuation of high-frequency S-waves has been demonstrated. The fact that gas is only present in relatively thin layers may explain why high frequency signals are subjected to a severe attenuation, whereas low frequency signals are almost unaffected. The source for the generation of gas is probably a layer with high organic content at a depth of approximately 25 m. The presence of gas is also suggested by an interval along the seismic line, where relatively low P-wave velocities are observed. In the same interval surprisingly high S-wave velocities and high shear strengths are present. The latter phenomena are presumably caused by precipitation of calcium carbonate at shallow depth. Whether the solution of calcium carbonate is caused by the presence of methane gas is uncertain.

Under the present project a spectral modelling technique for estimating synthetic seismogram in layered absorbing media has also been developed. The modelling technique is described and has been compared with a fourth order finite difference method. Almost the same solutions have been obtained by the two methods. The development has mainly concentrated on suppression of wrap-around effects, which cannot be avoided when discrete Fourier analysis is used. The periodic effects are considerably reduced by modifying the wave equation, so that an exponentially damped solution is determined. The artificial damping can be fully compensated for after the solution in the time-space domain has been found. By using this modelling technique relatively small period lengths can be employed, which ensures a fast modelling procedure. The present modelling technique has been used for evaluating the attenuation of high frequency reflection in the near surface layers with high gas content.

9 References

Båth, M., 1968, Mathematical Aspects of seismology, Elsevier, Amsterdam, pp 415.

Dyvik, R. and Madshus, C., 1985, Lab. measurements of G_{max} using bender elements. In: Advances in the art of testing soils under cyclic conditions, pp. 186-196, New York: American Society of Civil Engineers.

Ganley, D. C., 1981, A method for calculating synthetic seismograms which include the effect of absorption and dispersion, Geophysics 46, 1100-1107.

Jessen, A., 1936: Vendsyssels Geologi. Danm. geol. Unders., VRække, 2, 195 pp.

Jessen, A., Milthers, V., Nordmann, V., Hartz, N. & Hesselbo,A., 1910: En Boring gennem de kvartære Lag ved Skærumhede. Danm. geol. Unders., II Række, 25, 175 pp.

Kennett, B.L.N., 1979, Theoretical reflection seismograms for elastic media, Geophysical Prospecting 27, 301-321.

Levander, A.R., 1988, Fourth-order finite-difference P-SV seismograms, Geophysics 53, 1425-1436.

Liboriussen, J., Ashton, P. & Tygesen, T. 1987: The tectonicevolution of the Fennoscandian Border Zone in Denmark. Tectonophysics 137, 21-29.

Luke, K., 1994, The use of CPT in Danish soils with special emphasis on measuring the undrained shear strength, Ph.D. Thesis, ATV EF 368, Aalborg University.

Lykke-Andersen, A.-L., 1987: A Late Saalian, Eemian and Weichselian marine sequence at Nørre Lyngby, Vendsyssel, Denmark. Boreas 16, 345-357.

Moust Jacobsen, H., 1967, Morænelers geotekniske egenskaber. (The geotechnical properties of clay till), Ph.D. thesis 1967, Reprinted 1994, Aalborg University.

Moust Jacobsen, H., 1994, Svingninger i jord. Lærebog i videregående geoteknik 3. Aalborg University.

Nielsen, P.,H., 1978, Calculation of synthetic reflection seismograms in the frequency domain, Geophysical Prospecting 26, 399-406.

Nørmark, E., 1992. Residual static estimation by stack-power maximization in the frequency domain. Geophysical Prospecting 41, 551-563.

Stewart, W.P., and Campanella, R.G., 1993, Practical aspects of in situ measurements of material damping with the seismic cone penetration test, Canadian Geotechnical Journal 30, 211-219.

Thorsen, G. and Mortensen, P.K., 1995, CPT-investigations in young sediments in the northern part of Jutland, Proc. CPT'95, Linköping, pp. 317-322, Swedish Geotechnical Society Report 3:95.

Thorsen, G., 1996, Oedometer tests - an aid in determination of geological load history (in press).

AGEP: Engineering Geology papers

1 Lykke-Andersen, H., Thorsen, G., Hauerbach, P. (1996). Geotechnical and geological aspects of differential subsidence in the Skaw Spit, Denmark. Proc. NGM'96 Vol 1, pp 339-346, Reykjavik. Also in *AAU Geotechnical Engineering Papers*, ISSN 1398-6465 R9605.

2 Nörmark, E., Thorsen, G., Lykke-Andersen, H. (1996). Variations in acoustic properties of near surface sediments and the effects on high resolution seismic data evaluated by laboratory tests, in-situ measurements, and seismic modelling. (LITASEIS). Deutsche Wissenschaftliche Gesellschaft für Erdöl, Erdgas und Kohle e.V. DGMK Forschungsbericht 397-2/1. pp. 77-128. Also in *AAU Geotechnical Engineering Papers*, ISSN 1398-6465 R9609.